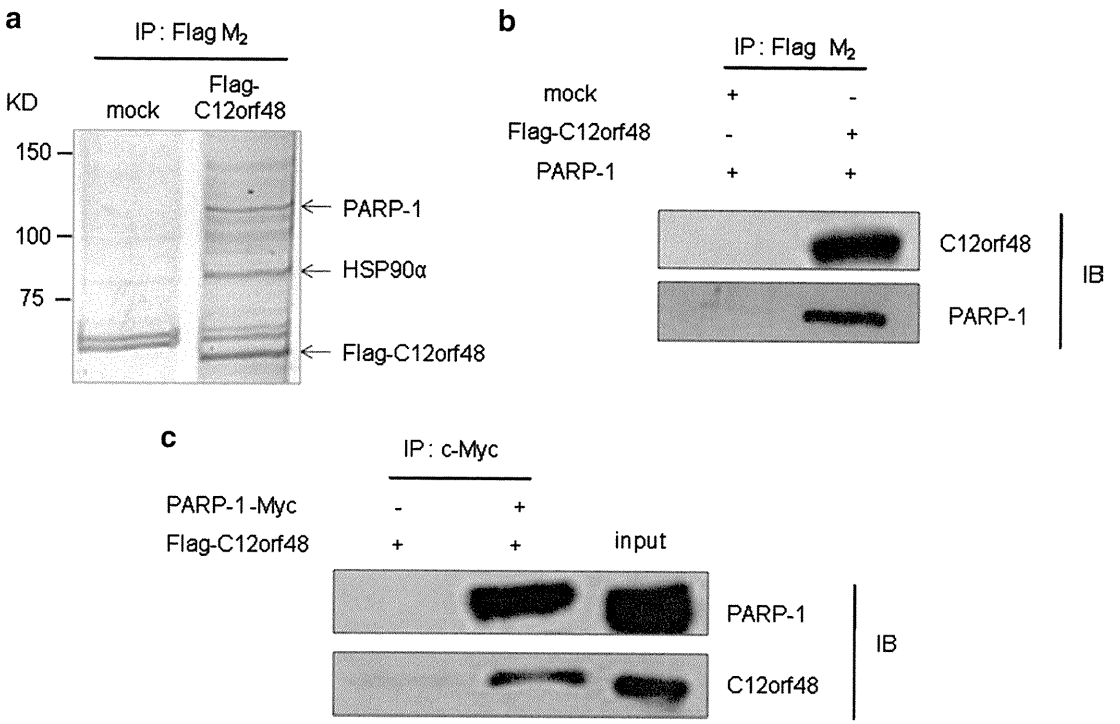

Figure 3. Identification of PARP-1 as an interacting protein of C12orf48. (a) Silver-staining of the immunoprecipitated complex separated on SDS-PAGE. Protein complexes were coimmunoprecipitated by anti-Flag M_2 agarose from the lysates of the HEK293 cells transfected with Flag-C12orf48 (right lane) or with mock (left lane). Two differential bands as well as Flag-C12orf48 (63 kD) were observed, and LC-MS/MS analysis identified PARP-1 (110 kD) and HSP90α (90 kD) as interacting proteins of C12orf48. (b) Western blot analysis using anti-PARP-1 antibody confirmed that PARP-1 protein was coimmunoprecipitated with Flag-C12orf48 protein. (c) Flag-C12orf48 expression vector was transfected to HEK293 cells without or with PARP-1-Myc expression vector. Cell lysates were immunoprecipitated by anti-Myc antibody. Flag-C12orf48 protein was coimmunoprecipitated with Myc-tagged PARP-1 protein.

recombinant C12orf48 protein in vitro. As shown in Figures 4a and 4b, we observed that addition of C12orf48 protein significantly enhanced the incorporation of [^{32}P]NAD^+ to recombinant PARP-1 protein in a dose-dependent manner when damaged DNA was coincubated, while this enhancement of PARP-1 automodification by C12orf48 was not observed in the absence of damaged DNA (data not shown). Furthermore, we transiently introduced C12orf48 into HEK293 cells and measured the PARP-1 activities in their lysates by the colorimetric PARP assay. In this experiment, PARP-1 in the cell extracts were activated by incubation with nicked DNA as described in Materials and Methods. As a result, we observed that PARP-1activities in the cell extracts were significantly enhanced by overexpression of C12orf48 (Fig. 4c).

Reduction of PARP-1 Activity by Depletion of C12orf48 in PDAC Cells

To examine the effect of C12orf48 on the PARP-1 activity in PDAC cells, we knocked down the expression of C12orf48 or PARP-1 itself in two PDAC cell lines, KLM-1 and SUIT-2, and measured the activities of PARP-1 in their cell lysates by the colorimetric PARP assay. The knockdown effects on C12orf48 and PARP-1 expression in KLM-1 and SUIT-2 cells were confirmed with anti-C12orf48 and anti-PARP-1 antibodies (Fig. 5a). Concordant with C12orf48 expression, the PARP-1 activities to modify histone H1 were decreased to 40.8 and 34.8% in C12orf48-depleted KLM-1 and SUIT-2 cells, respectively, compared with the control cells (Fig. 5b). The magnitude of this suppressive effect of C12orf48 on PARP-1 activity was almost same as the effect when PARP-1 itself was knocked down (Fig. 5b). Furthermore, we examined the level of poly(ADP-ribosyl)ation in the C12orf48-depleted cells by Western blot analysis using anti-poly (ADP-ribose) (PAR) antibody. As shown in Figure 5c, poly(ADP-ribosyl)ated proteins were detected at high molecular weights of more than 250 kD in the siEGFP-transfected control cells, while these poly(ADP-ribosyl)ation

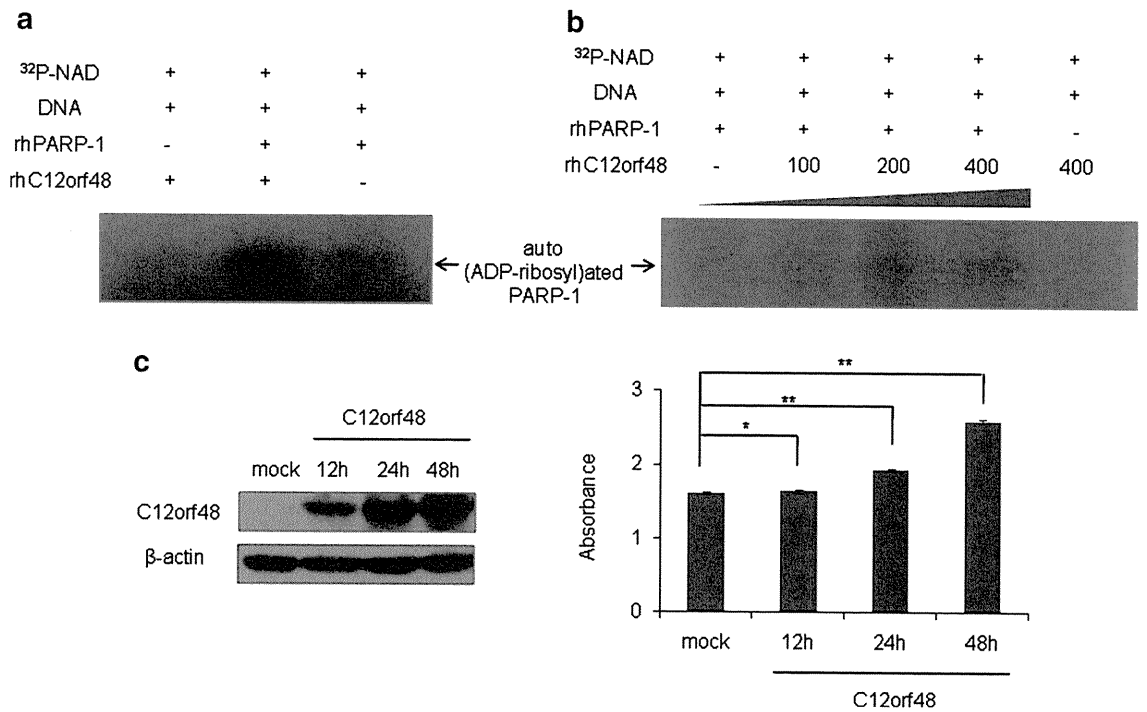

Figure 4. Regulation of PARP-1 activity by C12orf48. (a) Effect of C12orf48 on the auto(ADP-ribosyl)ation of PARP-1 in vitro. PARP-1 was automodified by incorporation of [^{32}P]NAD$^+$. Lane1, purified recombinant C12orf48 protein alone; lane2, both recombinant C12orf48 and recombinant PARP-1 protein; lane3, recombinant PARP-1 alone. (b) In vitro PARP-1 auto(ADP-ribosyl)ation was enhanced by increasing amount of recombinant C12orf48 protein. (c) HEK293 cells were transfected with C12orf48-expressing vector and harvested at indicated time points. The expression of C12orf48 was quantified by the immunoblot (left panel). The activities of PARP-1 to modify histone H1 were measured using the colorimetric PARP assays (right panel). These experiments were performed three times ($^*P < 0.05$, $^{**}P < 0.0001$, Student's t test).

was drastically reduced in the cells treated with C12orf48-siRNA or PARP-1-siRNA. PARP-1 is known to be the primary target for PARP-1-mediated (ADP-ribosyl)ation in vivo, with greater than 90% of PAR found on PARP-1 (Ogata et al., 1981; Huletsky et al., 1989; D'Amours et al., 1999). Automodified PARP-1 is detected clearly as a high-molecular form due to poly (ADP-riobse) formation. Therefore, it seemed that most of PAR proteins detected here were originated from auto(ADP-ribosyl)ated PARP-1. It suggested that depletion of C12orf48 could decrease PARP-1 enzymatic activity both in vivo and in vitro. In addition, depletion of PARP-1 by siRNA in KLM-1 and SUIT-2 cells (Supplementary Fig. 1) induced significant reduction in the number of viable cells. Together, these findings presumably explain that C12orf48 depletion lead to the reduction of pancreatic cancer cell viability, in part, through its direct interaction with PARP-1. However, it cannot be excluded that other C12orf48-specific and PARP1-independent effects can also affect cancer cell viability, and further study is required to clarify the roles of C12orf48 in cancer.

Sensitization of PDAC Cells to DNA Damage by C12orf48 Depletion

PARP-1 activity is relevant for the ability of cells to repair damaged DNA. It has been reported that inhibition of PARP-1 activity could increase the susceptibility of cells to DNA damaging agents (Daniel et al., 2009; Horton et al., 2009). Given the findings that C12orf48 could regulate PARP-1 activity, we assessed that the C12orf48 depletion could sensitize cancer cells to various DNA damaging agents. As expected, C12orf48-depleted KLM-1 cells showed much higher sensitivities to Adriamycin treatment, UV irradiation, and H_2O_2 treatment (Fig. 6a). These findings suggested that C12orf48 might protect cancer cells from cell death following the DNA damage or cellular stresses in cancer cells through the regulation of poly(ADP-ribosyl)ation activity of PARP-1.

Effect of C12orf48 in Cell-Cycle Checkpoint

Cell-cycle checkpoints are considered to facilitate DNA repair before entering the next cell-

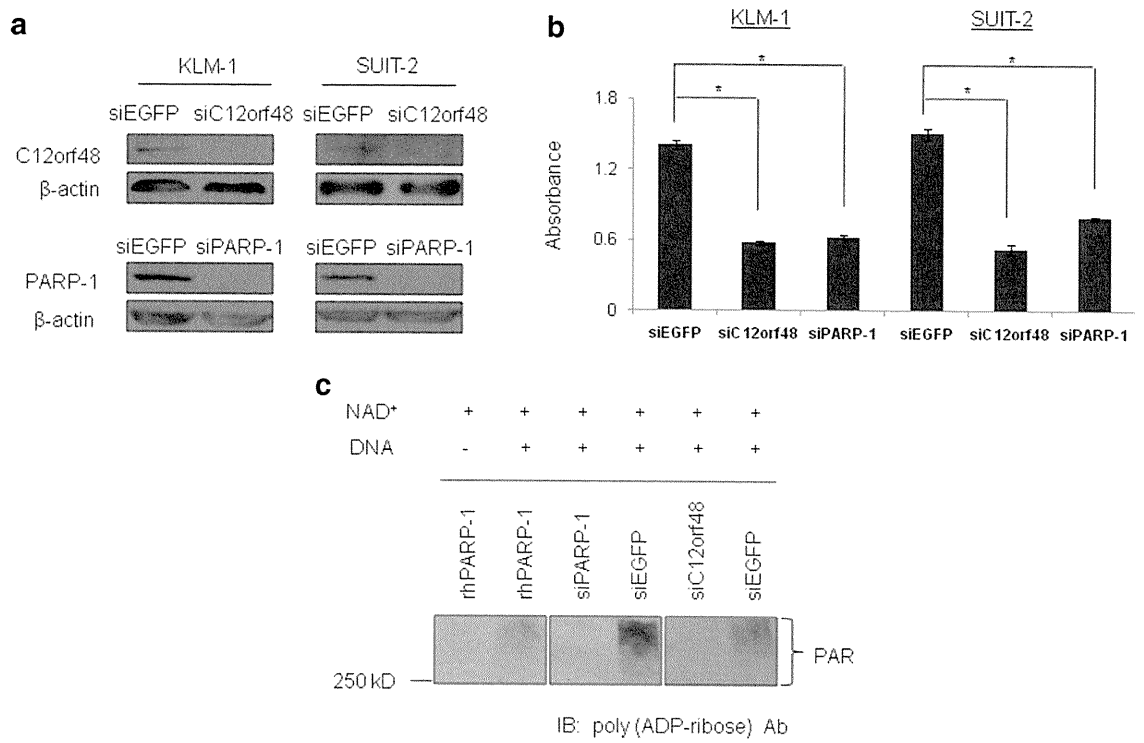

Figure 5. C12orf48-depletion reduced PARP-1 activity in PDAC cell extracts. (a) Western blot analysis using anti-C12orf48 and anti-PARP-1 antibodies confirmed knockdown effects of C12orf48 and PARP-1 expression in KLM-1 cells and SUIT-2 cells. (b) The activities of PARP-1 in the C12orf48-depleted or PARP-1-depleted cells were measured by the colorimetric PARP assays. *$P < 0.005$ by Student's t test. (c) PARP-1 enzymatic activities were investigated by anti-PAR antibody. Lane 1 and 2, recombinant PARP-1 protein; lane 3-6, KLM-1 cell extracts transfected with indicated siRNA. Automodified PARP-1 was detected at high molecular weights (>250 kD) only in the mixture with nicked DNA (Lane 2), but not the mixture without nicked DNA (Lane 1). Poly(ADP-ribosyl)ated proteins were observed at higher molecular weights (>250 kD) in the lysates of the siEGFP-transfected KLM-1 cells (Lanes 4 and 6). However, these poly(ADP-ribosyl)ation was diminished in the extracts of KLM-1 cells treated with PARP-1-siRNA (Lane 3) or C12orf48-siRNA (Lane 5).

cycle phases. Loss or attenuation of the checkpoint function may increase chances to cause gene mutations and chromosomal aberrations by affecting completion of the appropriate DNA repair. To test the effect of C12orf48 depletion on the cell-cycle progression, KLM-1 cells were synchronized at the G1-phase with aphidicolin treatment. After the release from the cell-cycle arrest, the cells depleted C12orf48 or PARP-1 entered into S-phase much faster than those treated with the control siEGFP (Fig. 6b). Six hours after the release from the arrest, approximately 73.3% of C12orf48-depleted cells and 75.7% of PARP1-depleted cells were already at S-phase. On the other hand, only 26.1% of the control cells (siEGFP) entered to S-phase. These findings indicated that depletion of C12orf48 or PARP-1 in PDAC cells could have some checkpoint dysfunction and resulted in very rapid progression from G1 to S-phase. We subsequently investigated the involvement of C12orf48 in the cell-cycle checkpoints after DNA damage by measuring the cell population at each cell-cycle phase after γ-irradiation. KLM-1 cells transfected with C12orf48-siRNA or siEGFP (as a control) were exposed to 3 Gy of γ-irradiation, and collected at various time-points after irradiation. Subsequent FACS analysis showed that C12orf48 depletion in KLM-1 cells enhanced G2/M arrest, compared with the control cells (Fig. 6c). Similarly, PARP-1 inhibitors were reported to enhance the G2 arrest after γ-irradiation (Nozaki et al., 1994). Taken together, our data implied that a decrease of PARP-1 activity in C12orf48-depleted cancer cells resulted in an enhancement of G2 arrest after γ-irradiation.

DISCUSSION

In this study, we focused on a novel gene *C12orf48*, one of the genes that were identified to be transactivated in PDAC cells through our genome-

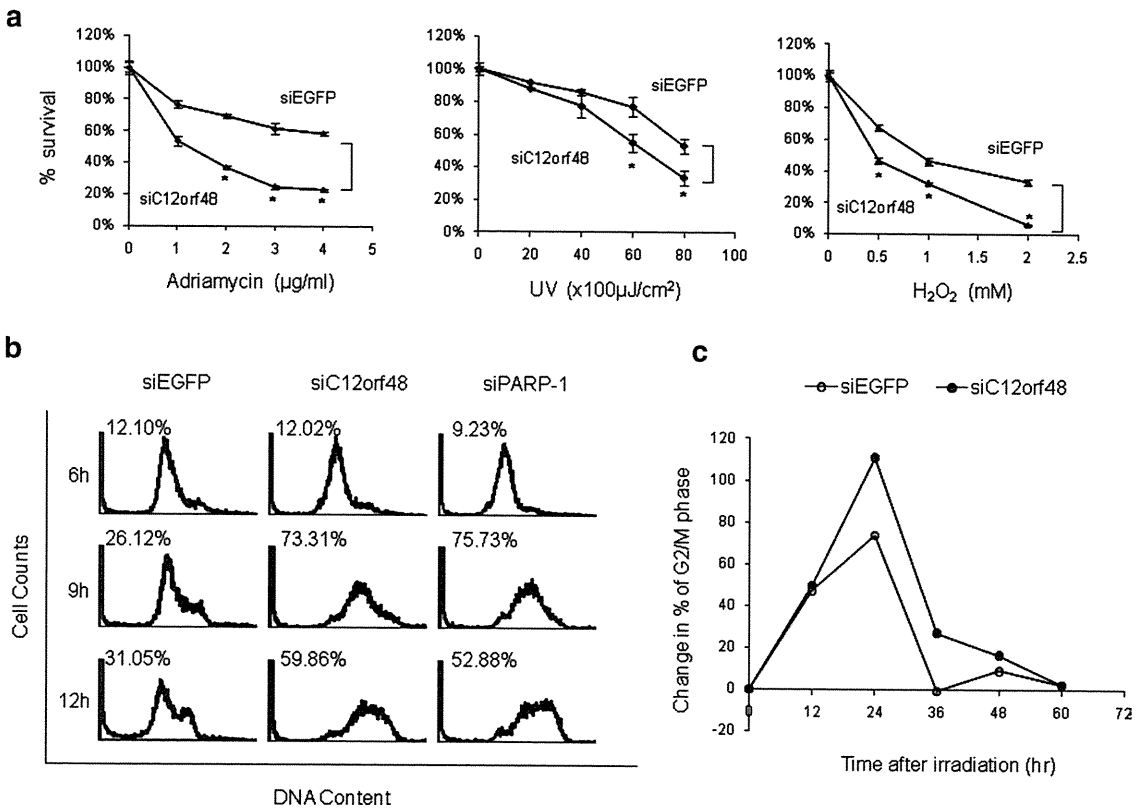

Figure 6. C12orf48-depletion sensitized PDAC cells to DNA damage. (a) The survival was reduced in the C12orf48-depleted KLM-1 cells after the exposure to DNA damaging agents. Data are shown as the averaged value from three experiments. *X*-axis represents the concentration of Adriamycin (left) and H_2O_2 (right) or the intensity of UV for DNA damaging. *Y*-axis represents the relative ratio of the cell numbers that was calculated in absorbance of the diameter by comparison with the absorbance value of damage-negative cells as a control. $^*P < 0.05$, by Student's *t* test. (b) FACS analysis demonstrated S-phase progression of synchronized KLM-1 cells. Cells were synchronized at G1-phase by aphidicolin treatment and released into S-phase by culturing in aphidicolin-free media. The population of S-phase was calculated. (c) The effects of C12orf48 depletion on the population of G2/M phase after γ-irradiation in KLM-1 cells. The KLM-1 cells with or without C12orf48 depletion were irradiated at the dose of 3 Gy, and then collected at the indicated time points for flow cytometry analysis. *X*-axis represents the time points after γ-radiation; *Y*-axis shows the relative population changes of G2/M phase by comparison with the G2/M population value of the KLM-1 cells without irradiation.

wide expression profile analysis (Nakamura et al., 2004). Its overexpression was also observed in other therapy-resistant malignancies, such as cholangiocarcinoma (Jinawath et al., 2006), castration-resistant prostate cancer (Tamura et al., 2007), and relapsed small-cell lung cancer (Taniwaki et al., 2006), indicating that it might be featured at therapy-resistant or aggresive malignancies. On the other hand, its expression was hardly detectable in any normal adult organs except the testis, implicating C12orf48 to be a cancer-testis antigen. Depletion of C12orf48 in some of PDAC cells resulted in significant reduction of cancer cell viability and survival, implying its critical roles in pancreatic carcinogenesis.

Importantly, we demonstrated that C12orf48 protein could physically interact with PARP-1 and positively regulate the enzymatic activity of PARP-1, suggesting that C12orf48, termed PARP-1 binding protein (PARPBP), might be involved in multiple cellular processes including DNA repair, chromatin modification, cell-cycle progression and genomic stability through the interaction and regulation of PARP-1. PARP-1, as a DNA nick-sensor, binds to DNA single-strand breaks (SSBs) and double-strand breaks (DSBs), and has an emerging and indispensable role in their repair. In regard to DNA damage signaling, PARP-1 is promptly stimulated and recruits the enzymes required for DNA repair to the site of DNA damage. Hence, the activity of PARP-1 plays a key role in signaling and initiating these processes. We demonstrated that C12orf48-depletion sensitized some of PDAC cells to DNA damage, suggesting that C12orf48 is likely to participate in the process of DNA repair through the regulation of PARP-1. Recent studies indicated that PARP-1 could be stimulated through

its binding to nucleosomes, and modulate chromatin structures (Kim et al., 2004). Although the underlying mechanisms of PARP-1 in the modulation of chromatin structure are largely unknown, our results indicate that C12orf48 could possibly be involved in the chromatin modulation as well. Hence, development of drugs inhibiting the interaction between C12orf48/PARPBP and PARP-1 should be a good therapeutic approach to achieve very specific cytotoxicy to some of pancreatic cancer cells with minimum risk of adverse effects to normal organs.

C12orf48 has no known functional motif or conserved domain. However, a previous study on a mouse homologue of C12orf48 protein suggested its high binding affinity to single-stranded DNA and polyA homopolymers (Borsu et al., 2000). Cell-cycle checkpoints are essentially critical to ensure the fidelity of cell division in cells for verification of each of the cell-cycle processes that need to be accurately completed before going into the next phase. In our studies, we showed that knockdown of C12orf48 as well as PARP-1 caused the failure of the G1/S cell-cycle checkpoint which would usually prevent the replication of cells having defects in DNA. Hence, this G1/S checkpoint failure induced by depletion of C12orf48 or PARP-1 in cancer cells could increase a possibility of accumulation of genetic mutations and/or genomic instability, resulting in growth retardation of cancer cells. Moreover, knockdown of C12orf48 in cancer cells enhanced G2/M arrest in PDAC cells after γ-irradiation, consistent with previous reports describing that PARP-1 inhibitors enhanced the G2 arrest after γ-irradiation (Nozaki et al., 1994). However, since the underlying mechanism of PARP-1 enzymatic activity in G2-arrest regulation is unclear, additional studies will be required to clarify it.

REFERENCES

Audebert M, Salles B, Calsou P. 2004. Involvement of poly(ADP-ribose) polymerase-1 and XRCC1/DNA ligase III in an alternative route for DNA double-strand breaks rejoining. J Biol Chem 279:55117–55126.

Audebert M, Salles B, Weinfeld M, Calsou P. 2006. Involvement of polynucleotide kinase in a poly(ADP-ribose) polymerase-1-dependent DNA double-strand breaks rejoining pathway. J Mol Biol 356:257–265.

Borsu L, Presse F, Nahon JL. 2000. The AROM gene, spliced mRNAs encoding new DNA/RNA-binding proteins are transcribed from the opposite strand of the melanin-concentrating hormone gene in mammals. J Biol Chem 275:40576–40587.

D'Amours D, Desnoyers S, D'Silva I, Poirier GG. 1999. Poly(ADP-ribosyl)ation reactions in the regulation of nuclear functions. Biochem J 342:249–268.

D'Silva I, Pelletier JD, Lagueux J, D'Amours D, Chaudhry MA, Weinfeld M, Lees-Miller SP, Poirier GG. 1999. Relative affinities of poly(ADP-ribose) polymerase and DNA-dependent protein kinase for DNA strand interruptions. Biochim Biophys Acta 1430:119–126.

Daniel RA, Rozanska AL, Thomas HD, Mulligan EA, Drew Y, Castelbuono DJ, Hostomsky Z, Plummer ER, Boddy AV, Tweddle DA, Curtin NJ, Clifford SC. 2009. Inhibition of poly-(ADP-ribose) polymerase-1 enhances temozolomide and topotecan activity against childhood neuroblastoma. Clin Cancer Res 15:1241–1249.

Dantzer F, de La Rubia G, Menissier-De Murcia J, Hostomsky Z, de Murcia G, Schreiber V. 2000. Base excision repair is impaired in mammalian cells lacking poly(ADP-ribose) polymerase-1. Biochemistry 39:7559–7569.

de Murcia G, Ménissier de Murcia J. 1994. Poly(ADP-ribose) polymerase: A molecular nick-sensor. Trends Biochem Sci 19:172–176.

Di Palma T, de Cristofaro T, D'Ambrosio C, Del Prete D, Scaloni A, Zannini M. 2008. Poly(ADP-ribose) polymerase 1 binds to Pax8 and inhibits its transcriptional activity. J Mol Endocrinol 41:379–388.

DiMagno EP, Reber HA, Tempero MA. 1999. AGA technical review on the epidemiology, diagnosis, and treatment of pancreatic ductal adenocarcinoma. Gastroenterology 117:1464–1484.

Durkacz BW, Omidiji O, Gray DA, Shall S. 1980. (ADP-ribose)n participates in DNA excision repair. Nature 283:593–596.

Hoeijmakers JH. 2001. Genome maintenance mechanisms for preventing cancer. Nature 411:366–374.

Horton TM, Jenkins G, Pati D, Zhang L, Dolan ME, Ribes-Zamora A, Bertuch AA, Blaney SM, Delaney SL, Hegde M, Berg SL. 2009. Poly(ADP-ribose) polymerase inhibitor ABT-888 potentiates the cytotoxic activity of temozolomide in leukemia cells: Influence of mismatch repair status and O6-methylguanine-DNA methyltransferase activity. Mol Cancer Ther 8:2232–2242.

Hosokawa M, Takehara A, Matsuda K, Eguchi H, Ohigashi H, Ishikawa O, Shinomura Y, Imai K, Nakamura Y, Nakagawa H. 2007. Oncogenic role of KIAA0101 interacting with proliferating cell nuclear antigen in pancreatic cancer. Cancer Res 67:2568–2576.

Hosokawa M, Kashiwaya K, Eguchi H, Ohigashi H, Ishikawa O, Furihata M, Shinomura Y, Imai K, Nakamura Y, Nakagawa H. 2008. Over-expression of cysteine proteinase inhibitor cystatin 6 promotes pancreatic cancer growth. Cancer Sci 99:1626–1632.

Huletsky A, de Murcia G, Muller S, Hengartner M, Ménard L, Lamarre D, Poirier GG. 1989. The effect of poly(ADP-ribosyl)ation on native and H1-depleted chromatin. A role of poly(ADP-ribosyl)ation on core nucleosome structure. J Biol Chem 264:8878–8886.

Iizumi M, Hosokawa M, Takehara A, Chung S, Nakamura T, Katagiri T, Eguchi H, Ohigashi H, Ishikawa O, Nakamura Y, Nakagawa H. 2006. EphA4 receptor, overexpressed in pancreatic ductal adenocarcinoma, promotes cancer cell growth. Cancer Sci 97:1211–1216.

Jemal A, Siegel R, Ward E, Hao Y, Xu J, Thun MJ. 2009. Cancer statistics, 2009. CA Cancer J Clin 59:225–249.

Jinawath N, Chamgramol Y, Furukawa Y, Obama K, Tsunoda T, Sripa B, Pairojkul C, Nakamura Y. 2006. Comparison of gene expression profiles between *Opisthorchis viverrini* and non-*Opisthorchis viverrini* associated human intrahepatic cholangiocarcinoma. Hepatology 44:1025–1038.

Jones P, Altamura S, Boueres J, Ferrigno F, Fonsi M, Giomini C, Lamartina S, Monteagudo E, Ontoria JM, Orsale MV, Palumbi MC, Pesci S, Roscilli G, Scarpelli R, Schultz-Fademrecht C, Toniatti C, Rowley M. 2009. Discovery of 2-{4-[(3S)-piperidin-3-yl]phenyl}-2H-indazole-7-carboxamide (MK-4827): A novel oral poly(ADP-ribose)polymerase (PARP) inhibitor efficacious in BRCA-1 and -2 mutant tumors. J Med Chem 52:7170–7185.

Kameshita I, Matsuda Z, Taniguchi T, Shizuta Y. 1984. Poly (ADP-ribose) synthetase. Separation and identification of three proteolytic fragments as the substrate-binding domain, the DNA-binding domain, and the automodification domain. J Biol Chem 259:4770–4776.

Kashiwaya K, Hosokawa M, Eguchi H, Ohigashi H, Ishikawa O, Shinomura Y, Nakamura Y, Nakagawa H. 2009. Identification of C2orf18, termed ANT2BP (ANT2-binding protein), as one of the key molecules involved in pancreatic carcinogenesis. Cancer Sci 100:457–464.

Kim MY, Mauro S, Gévry N, Lis JT, Kraus WL. 2004. NAD^+-dependent modulation of chromatin structure and transcription by nucleosome binding properties of PARP-1. Cell 119:803–814.

Longley DB, Johnston PG. 2005. Molecular mechanisms of drug resistance. J Pathol 205:275–292.

Miknyoczki S, Chang H, Grobelny J, Pritchard S, Worrell C, McGann N, Ator M, Husten J, Deibold J, Hudkins R, Zulli A, Parchment R, Ruggeri B. 2007. The selective poly(ADP-ribose) polymerase-1(2) inhibitor, CEP-8983, increases the sensitivity of chemoresistant tumor cells to temozolomide and irinotecan but does not potentiate myelotoxicity. Mol Cancer Ther 6:2290–2302.

Nakamura T, Furukawa Y, Nakagawa H, Tsunoda T, Ohigashi H, Murata K, Ishikawa O, Ohgaki K, Kashimura N, Miyamoto M, Hirano S, Kondo S, Katoh H, Nakamura Y, Katagiri T. 2004. Genome-wide cDNA microarray analysis of gene-expression profiles in pancreatic cancers using populations of tumor cells and normal ductal epithelial cells selected for purity by laser microdissection. Oncogene 23:2385–2400.

Nozaki T, Masutani M, Akagawa T, Sugimura T, Esumi H. 1994. Suppression of G1 arrest and enhancement of G2 arrest by inhibitors of poly(ADP-ribose) polymerase: Possible involvement of poly(ADP-ribosyl)ation in cell cycle arrest following gamma-irradiation. Jpn J Cancer Res 85:1094–1098.

O'Shaughnessy J, Osborne C, Pippen J, Yoffe M, Patt D, Monaghan G, Rocha C, Ossovskaya V, Sherman B, Bradley C. 2009. Efficacy of BSI-201, a poly (ADP-ribose) polymerase-1 (PARP1) inhibitor, in combination with gemcitabine/carboplatin (G/C) in patients with metastatic triple-negative breast cancer (TNBC): Results of a randomized phase II trial. J Clin Oncol 27:3.

Ogata N, Ueda K, Kawaichi M, Hayaishi O. 1981. Poly(ADP-ribose) synthetase, a main acceptor of poly(ADP-ribose) in isolated nuclei. J Biol Chem 256:4135–4137.

Plummer R, Jones C, Middleton M, Wilson R, Evans J, Olsen A, Curtin N, Boddy A, McHugh P, Newell D, Harris A, Johnson P, Steinfeldt H, Dewji R, Wang D, Robson L, Calvert H. 2008. Phase I study of the poly(ADP-ribose) polymerase inhibitor, AG014699, in combination with temozolomide in patients with advanced solid tumors. Clin Cancer Res 14:7917–7923.

Rottenberg S, Jaspers JE, Kersbergen A, van der Burg E, Nygren AO, Zander SA, Derksen PW, de Bruin M, Zevenhoven J, Lau A, Boulter R, Cranston A, O'Connor MJ, Martin NM, Borst P, Jonkers J. 2008. High sensitivity of BRCA1-deficient mammary tumors to the PARP inhibitor AZD2281 alone and in combination with platinum drugs. Proc Natl Acad Sci USA 105:17079–17084.

Takehara A, Eguchi H, Ohigashi H, Ishikawa O, Kasugai T, Hosokawa M, Katagiri T, Nakamura Y, Nakagawa H. 2006. Novel tumor marker REG4 detected in serum of patients with resectable pancreatic cancer and feasibility for antibody therapy targeting REG4. Cancer Sci 97:1191–1197.

Takehara A, Hosokawa M, Eguchi H, Ohigashi H, Ishikawa O, Nakamura Y, Nakagawa H. 2007. Gamma-aminobutyric acid (GABA) stimulates pancreatic cancer growth through overexpressing GABAA receptor pi subunit. Cancer Res 67:9704–9712.

Tamura K, Furihata M, Tsunoda T, Ashida S, Takata R, Obara W, Yoshioka H, Daigo Y, Nasu Y, Kumon H, Konaka H, Namiki M, Tozawa K, Kohri K, Tanji N, Yokoyama M, Shimazui T, Akaza H, Mizutani Y, Miki T, Fujioka T, Shuin T, Nakamura Y, Nakagawa H. 2007. Molecular features of hormone-refractory prostate cancer cells by genome-wide gene-expression profiles. Cancer Res 67:5117–5125.

Taniuchi K, Nakagawa H, Hosokawa M, Nakamura T, Eguchi H, Ohigashi H, Ishikawa O, Katagiri T, Nakamura Y. 2005a. Overexpressed P-cadherin/CDH3 promotes motility of pancreatic cancer cells by interacting with p120ctn and activating rho-family GTPases. Cancer Res 65:3092–3099.

Taniuchi K, Nakagawa H, Nakamura T, Eguchi H, Ohigashi H, Ishikawa O, Katagiri T, Nakamura Y. 2005b. Down-regulation of RAB6KIFL/KIF20A, a kinesin involved with membrane trafficking of discs large homologue 5, can attenuate growth of pancreatic cancer cell. Cancer Res 65:105–112.

Taniwaki M, Daigo Y, Ishikawa N, Takano A, Tsunoda T, Yasui W, Inai K, Kohno N, Nakamura Y. 2006. Gene expression profiles of small-cell lung cancers: Molecular signatures of lung cancer. Int J Oncol 29:567–575.

Wang M, Wu W, Wu W, Rosidi B, Zhang L, Wang H, Iliakis G. 2006. PARP-1 and Ku compete for repair of DNA double strand breaks by distinct NHEJ pathways. Nucleic Acids Res 34:6170–6182.

Wray CJ, Ahmad SA, Matthews JB, Lowy AM. 2005. Surgery for pancreatic cancer: Recent controversies and current practice. Gastroenterology 128:1626–1641.

nature COMMUNICATIONS

ARTICLE

Received 5 Dec 2011 | Accepted 11 Jan 2012 | Published 14 Feb 2012

DOI: 10.1038/ncomms1676

Regulation of histone modification and chromatin structure by the p53–PADI4 pathway

Chizu Tanikawa[1], Martha Espinosa[1,2], Akari Suzuki[3], Ken Masuda[1], Kazuhiko Yamamoto[3,4], Eiju Tsuchiya[5,6], Koji Ueda[7], Yataro Daigo[1,8], Yusuke Nakamura[1] & Koichi Matsuda[1]

Histone proteins are modified in response to various external signals; however, their mechanisms are still not fully understood. Citrullination is a post-transcriptional modification that converts arginine in proteins into citrulline. Here we show *in vivo* and *in vitro* citrullination of the arginine 3 residue of histone H4 (cit-H4R3) in response to DNA damage through the p53–PADI4 pathway. We also show DNA damage-induced citrullination of Lamin C. Cit-H4R3 and citrullinated Lamin C localize around fragmented nuclei in apoptotic cells. Ectopic expression of PADI4 leads to chromatin decondensation and promotes DNA cleavage, whereas *Padi4*$^{-/-}$ mice exhibit resistance to radiation-induced apoptosis in the thymus. Furthermore, the level of cit-H4R3 is negatively correlated with p53 protein expression and with tumour size in non-small cell lung cancer tissues. Our findings reveal that cit-H4R3 may be an 'apoptotic histone code' to detect damaged cells and induce nuclear fragmentation, which has a crucial role in carcinogenesis.

[1] Laboratory of Molecular Medicine, Human Genome Center, Institute of Medical Science, The University of Tokyo, Tokyo 1088639, Japan. [2] Department of Infectomics and Molecular Pathogenesis, Center for Research and Advanced Studies, Mexico City 07360, Mexico. [3] Laboratory for Rheumatic Diseases, Center for Genomic Medicine, RIKEN, Yokohama 2300045, Japan. [4] Department of Allergy and Rheumatology, Graduate School of Medicine, the University of Tokyo, Tokyo 1138655 Japan. [5] Department of Pathology, Saitama Cancer Center, Saitama 3620806, Japan. [6] Molecular Pathology and Genetics Division, Kanagawa Cancer Center Research Institute, Kanagawa 2418515, Japan. [7] Laboratory for Biomarker Development, Center for Genomic Medicine, RIKEN, Yokohama 2300045, Japan. [8] Department of Medical Oncology, Shiga University of Medical Science, Otsu 5202192, Japan. Correspondence and requests for materials should be addressed to K.M. (email: koichima@ims.u-tokyo.ac.jp).

24

In response to DNA damage, various protein kinases phosphorylate p53 at its amino terminus leading to the stabilization and accumulation of p53 protein[1,2]. As a guardian of the genome, p53 transactivates a number of its target genes to induce cell-cycle arrest or apoptosis and subsequently eliminates cells with risk of malignant transformation[3]. Morphological changes such as chromatin condensation, DNA laddering, nuclear lamina breakdown and nuclear fragmentation are characteristic of apoptotic cell death, although the role of p53 during these dynamic nuclear events has not been elucidated.

We have isolated a number of p53-target genes including p53AIP1, p53R2, p53RDL1 and XEDAR[4–9], and implicated the molecular mechanisms by which p53 regulated the cell fate, death or survival, by regulating the expression levels of these genes. We recently reported a p53-regulated posttranscriptional modification of many proteins through the transcriptional regulation of PADI4 (ref. 10) that converts an arginine residue in proteins to a citrulline residue, known as citrullination or deimination[11]. This reaction is mediated by the Ca^{2+}-dependent enzyme peptidylarginine deiminase. Citrullination of proteins causes a loss of positive charge and results in a significant biochemical effect. Bacterial infection has been indicated to stimulate PADI4-mediated hypercitrullination of histones in neutrophils and subsequently promoted highly decondensed extracellular chromatin structure called NET (neutrophil extracellular trap) that could capture and kill microorganisms[12,13]. On the other hand, citrullinated peptides/proteins are recognized as non-self proteins and subsequently activate immune systems. Citrullinated myelin basic protein in the brain is considered as a putative autoantigen associated with multiple sclerosis[14]. In addition, autoantibodies against citrullinated peptides derived

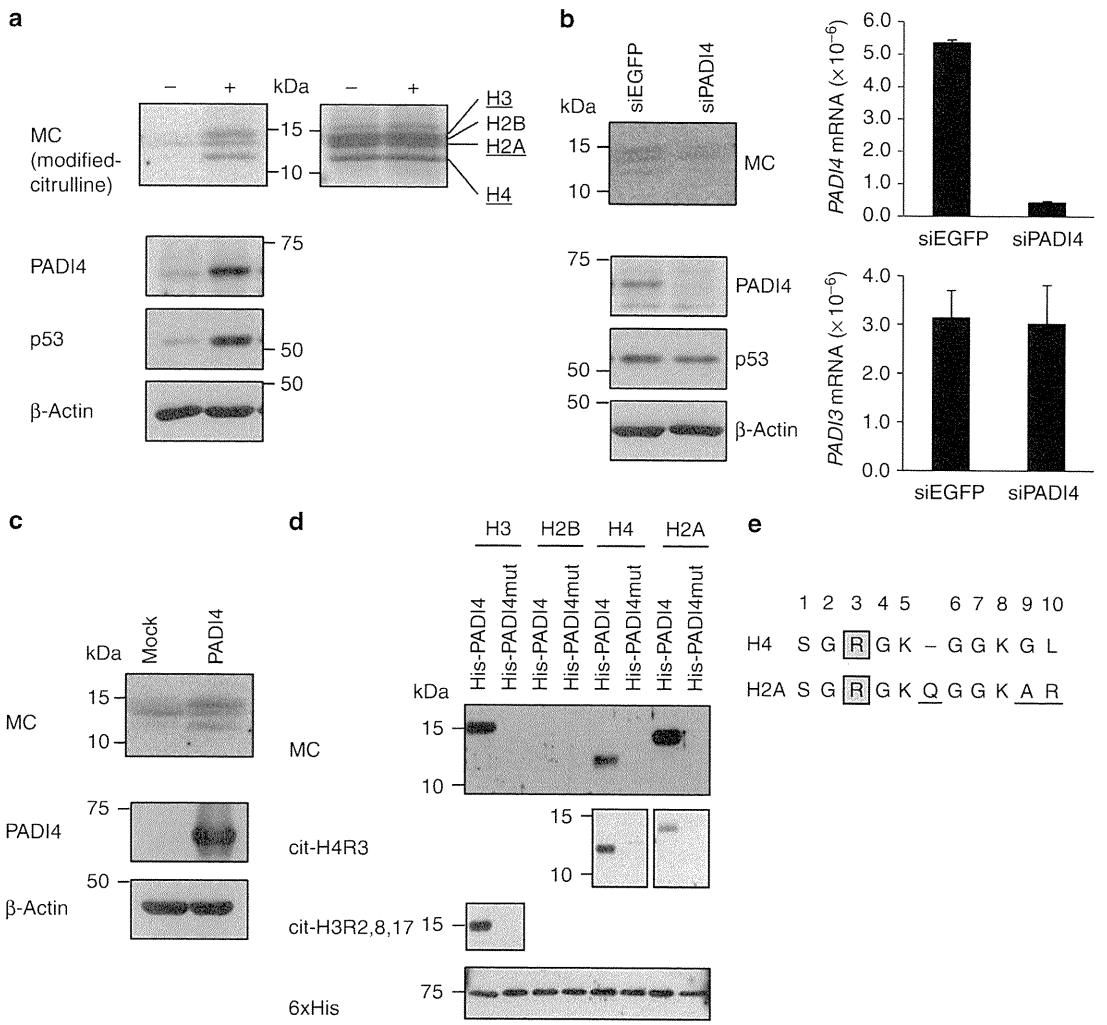

Figure 1 | Citrullination of core histones in the damaged cells. (**a**) Histones extracted from U-2 OS cells 48 h after ADR treatment (lane 2) were immunoblotted with anti-modified citrulline (anti-MC) antibody (left panel). U-2 OS cells without ADR treatment were used as a negative control (lane 1). CBB stain is shown in the right panel to ensure equal loading. Whole-cell extracts were subjected to immunoblotting with anti-PADI4, anti-p53 or anti-β-actin antibody. (**b**) siRNA against PADI4 was trasfected 10 h before DNA damage treatment. siEGFP was used as a control. Purified histones were immunoblotted with anti-MC antibody (upper left panel). Whole-cell extracts were subjected to immunoblotting with anti-PADI4, anti-p53 or anti-β-actin antibody (lower left panel). Quantitative PCR analysis of *PADI4* or *PADI3* expression (right panel). Error bars represent range ($n = 2$). *GAPDH* was used for normalization of expression levels. (**c**) Histones were extracted from PADI4-introduced or mock-transfected HEK293T cells, and immunoblotted with anti-MC antibody. Whole-cell extracts were subjected to immunoblotting with anti-PADI4 or anti-β-actin antibody. (**d**) *In vitro* citrullination followed by western blotting with anti-MC, anti-citrullinated histone H4R3 (cit-H4R3), anti-citrullinated histone H3R2,8,17 (cit-H3R2,8,17), or anti-His-tag (6×His) antibody. Each recombinant histone was incubated with wild-type or mutant PADI4 protein in the presence of 10^{-3} M of calcium at 37 °C for 1 h. (**e**) Alignment of amino-acid sequences of the N-terminal regions of histones H2A and H4.

from filaggrin or fibrin have been established as specific markers for rheumatoid arthritis[15–17]. Furthermore, we have revealed that a functional haplotype of the *PADI4* gene is associated with rheumatoid arthritis[18]. Thus, activated PADI4 function has been shown to be associated with the pathogenesis of rheumatoid arthritis through induction of the antigenicity of proteins. Here we investigate the physiological role of p53–PADI4 signalling in the DNA damage response by using PADI4 deficient mice as well as clinical cancer tissues. In this study, we revealed the crucial role of PADI4 in the apoptotic pathway and human carcinogenesis.

Results

Citrullination of core histones in response to DNA damage. As histones H3 and H4 were shown to be citrullinated by PADI4 (refs 19,20), we assessed whether core histones are citrullinated in response to DNA damage. Acid-extracted histones from adriamycin (ADR)-treated U-2 OS cells were immunoblotted with an antibody against a chemically modified form of citrulline (anti-MC antibody). Western blot analysis revealed the citrullination of three of four core histones in a PADI4-dependent manner (Fig. 1a,b). Ectopic expression of PADI4 also induced the citrullination of at least two core histones (Fig. 1c). To further characterize this modification, purified histones were treated with recombinant PADI4. Antibodies against specific citrulline residues (cit-H3R2,8,17 or cit-H4R3) as well as anti-MC antibody could detect PADI4-treated histones H3 and H4, respectively (Fig. 1d). Interestingly, anti-cit-H4R3 antibody cross-reacted with citrullinated H2A, probably owing to the high similarity between histones H4 and H2A (Fig. 1d,e).

p53–PADI4 citrullinates histone H4R3. Western blotting of core histone proteins purified from ADR-treated U-2 OS cells indicated citrullination of H4R3 by DNA damage (Fig. 2a), but the citrullination was blocked by small interfering RNA (siRNA) against p53 or PADI4 (Fig. 2b). Concordantly, ectopic introduction of PADI4 into cells induced the citrullination of H4R3 (Fig. 2c). Although PADI4 was reported to function as demethylase of mono-methyl-H4R3 *in vitro*[19,20], PADI4 activation did not affect H4R3 methylation status in our experimental system (Supplementary Fig. S1).

We also found the citrullination of histone H3 at its N terminus in non-treated U-2 OS cells and HEK293T cells (Supplementary Fig. S1), but these modifications were hardly detectable with anti-MC antibody, probably because of the low sensitivity of this antibody to the citrullination at its N terminus of histone H3 (Fig. 1a,c). Although citrullination of H3 was slightly increased by ectopic expression of PADI4 or by ADR treatment, siPADI4 did not affect H3-citrullination level (Supplementary Fig. S1). Because citrullination of H3 was observed in HEK293T and U-2 OS cells without any stresses, we suspect that other PADI family members might also be involved in H3 citrullination in these cells.

Localization of citrullinated histone H4 at fragmented nuclei. To investigate the physiological role of PADI4-mediated histone citrullination, we examined chromatin structure and subcellular localization of cit-H4R3 in PADI4-introduced HEK293T cells. Immunocytochemical analysis revealed the weak and irregular staining of nuclei with 4,6-diamidino-2-phenylindole (DAPI), a characteristic feature of chromatin decondensation (Fig. 3a). In contrast, cit-H4R3 displayed a dot-like staining pattern around the decondensed nuclei in cells expressing HA-PADI4 (Fig. 3a). Fractionation of chromatin obtained from PADI4-introduced HEK293T cells[21] suggested that cit-H4R3 was enriched in S1 (soluble in divalent metal; transcriptional active) and S2 (soluble in EDTA; transcriptional inactive) fractions, compared with P fraction (insoluble compact chromatin) (Fig. 3b). As apoptosis is associated with dynamic changes of nuclear structure, we examined the localization cit-H4R3 in apoptotic cells. At 48 h after treatment with ADR, cit-H4R3 was localized around the fragmented nuclei in U-2 OS cells, but it was not detected in the cells, additionally treated with siRNA against PADI4 (Fig. 3c,d). Similar results were observed in ADR-treated MCF7 cells (Supplementary Fig. S2a,b). In addition, cit-H4R3 expression was significantly correlated with the level of apoptosis induction demonstrated by the TdT-mediated dUTP nick

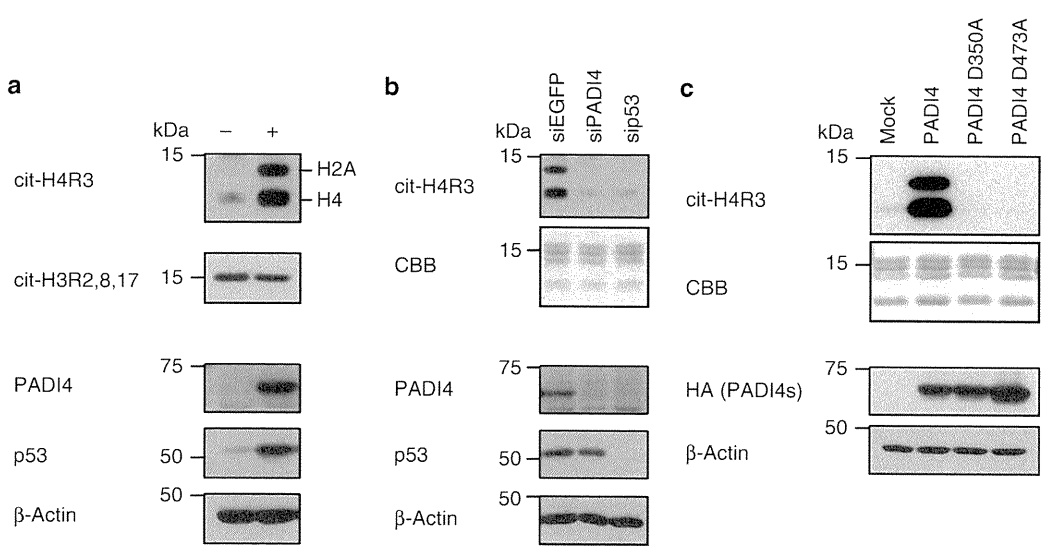

Figure 2 | Citrullination of histone H4R3 in the damaged cells. (**a**) Western blotting for histones extracted from ADR-treated U-2 OS cells (lane 2) using antibodies against citrullinated histone H4R3 (cit-H4R3) or citrullinated histone H3R2,8,17 (cit-H3R2,8,17). Whole-cell extracts were subjected to immunoblotting with anti-PADI4, anti-p53 or anti-β-actin antibody. U-2 OS cells without ADR treatment were used as a control (lane 1). (**b**) siRNA against PADI4 or p53 was transfected 10 h before ADR treatment. siEGFP was used as a control. Extracted histones were immunoblotted with anti-cit-H4R3 antibody. Whole-cell extracts were subjected to immunoblotting with anti-PADI4, anti-p53 or anti-β-actin antibody. CBB staining was shown to ensure equal loading. (**c**) Histones were extracted from HEK293T cells transfected with plasmid-expressing HA tagged-wild-type PADI4, mutant PADI4 (D350A or D473A), or mock and immunoblotted with anti-cit-H4R3 antibody. Whole-cell extracts were subjected to immunoblotting with anti-HA or anti-β-actin antibody.

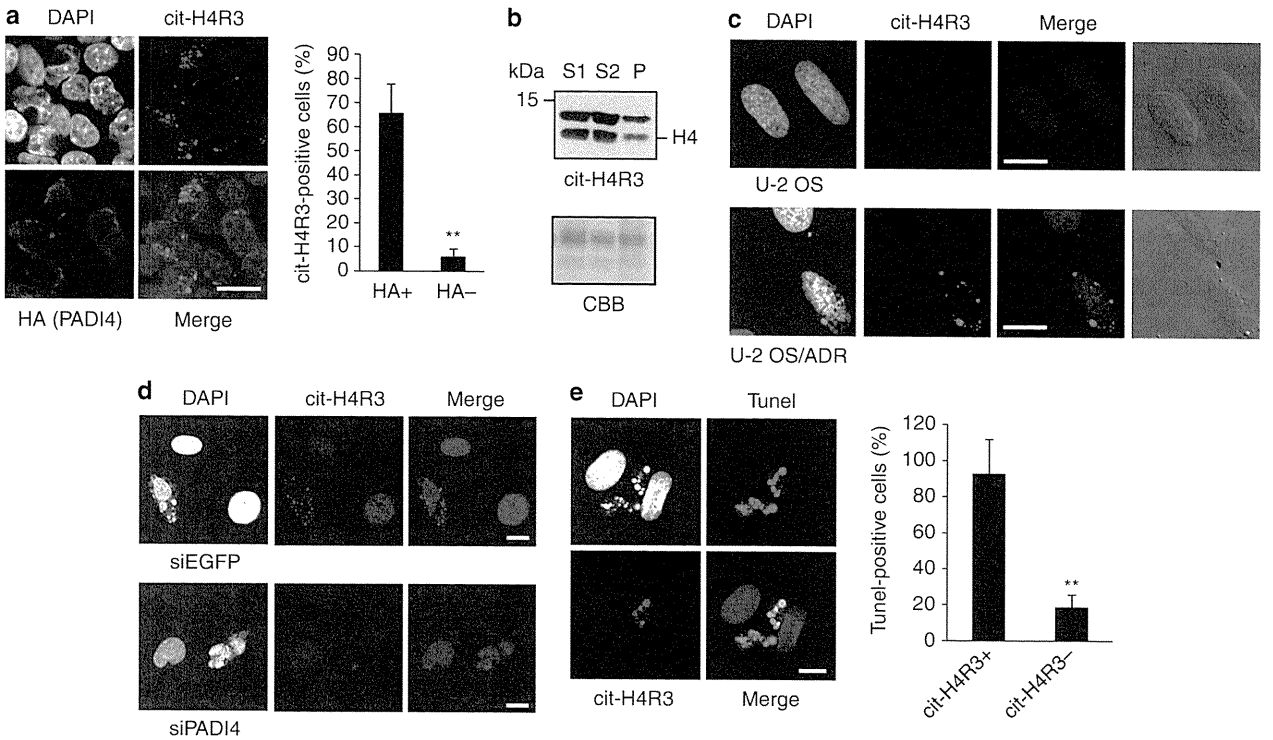

Figure 3 | Localization of cit-H4R3 around the fragmented nuclei during apoptosis. (**a**) Representative image of HA-PADI4-transfected HEK293T cells stained with anti-citrullinated histone H4R3 (cit-H4R3) antibody (Alexa Fluor 488) and anti-HA antibody (Aleza Fluor 594) (left panel).The proportion of cit-H4R3-positive cells stratified by HA-PADI4 expression was indicated (right panel). Error bars represent s.d. ($n=4$). $^{**}P<0.01$ by Student's t-test. Scale bars, 20 μm. (**b**) Chromatin fractionation followed by western blotting. Isolated nuclei from HEK293T cells transfected with PADI4-expressing plasmids were digested with MNase. Digested nuclei were fractionated into three fractions: transcriptionally active (S1), transcriptionally inactive (S2) and insoluble compact chromatin (P). Aliquots from S1, S2 and P fractions were separated by SDS-PAGE and then analysed by western blotting using anti-cit-H4R3 antibody. (**c**) Representative image of ADR-treated U-2 OS cells stained with anti-cit-H4R3 antibody (Alexa Fluor 488). Cells were treated with 2 μg ml^{-1} of ADR for 2 h and fixed 48 h later. Scale bars, 20 μm. (**d**) Representative image of ADR-treated U-2 OS cells stained with anti-citrullinated histone H4R3 antibody (Alexa Fluor 488). Each cell line was treated with 2 μg ml^{-1} of ADR for 2 h and fixed 48 h later. Each siRNA was transfected 10 h before the ADR treatment. siEGFP was used as a control. Scale bars, 20 μm. (**e**) Co-staining of U-2 OS cells with TUNEL (FITC) and anti-cit-H4R3 antibody (Alexa Fluor 594) at 48 h after treatment with 2 μg ml^{-1} of ADR for 2 h (left panel). The proportion of TUNEL positive cells stratified by cit-H4R3 expression was indicated (right panel). Error bars represent s.d. ($n=7$). $^{**}P<0.01$ by Student's t-test. Scale bars, 20 μm.

end labeling (TUNEL) assay in ADR-treated U-2 OS cells (Fig. 3e). These findings indicated that cit-H4R3 was associated with the decondensed soluble chromatin in apoptotic cells.

PADI4 promotes DNA fragmentation. In neutrophils, histone hypercitrullination is known to mediate NET formation that is associated with highly decondensed chromatin structures[22]. As chromatin decondensation was shown to increase the accessibility of DNase, we hypothesized that PADI4 promotes nuclear fragmentation. Micrococcal nuclease (MNase), which can digest chromatin at the linker DNA region into solubilized poly- and mono-nucleosome-size fragments, was used to evaluate the accessibility of DNA as well as chromatin compaction. MNase treatment of purified chromatin produced fragmented-nucleosomes more effectively in cells transfected with wild-type PADI4 than those with mutant PADI4 or mock (Fig. 4a). This result was confirmed by SDS–PAGE in which core histones from soluble nucleosome were stained with Coomassie brilliant blue (CBB) (Fig. 4b). ADR treatment also enhanced DNA cleavage (evaluated by histones in soluble nucleosome), but pretreatment with the siPADI4 remarkably suppressed MNase-mediated DNA digestion (Fig. 4c). Taking these observations into account, our findings revealed that PADI4 increased the accessibility of DNA and subsequently promoted the DNA fragmentation.

p53–PADI4 citrullinates Lamin C at its carboxy terminus. Next, we introduced PADI4 into HEK293T cells and performed immunocytochemical analysis using anti-MC antibody. The results clearly indicated the citrullination of nuclear membrane proteins in cells expressing HA-PADI4 (Fig. 5a). Lamin family proteins are the main components of the nuclear lamina and are essential for various nuclear processes including apoptosis. Western blotting using nuclear extracts from PADI4-introduced HEK293T cells revealed the band shift of Lamin C protein, but not those of other Lamin proteins (Fig. 5b). Furthermore, we detected the citrullination of immunopurified Lamin C protein from PADI4-introduced HEK293T cells using anti-MC antibody (Fig. 5c). Because Lamins A and C share 566 amino acids of their N-terminal portions, six carboxy-terminal amino acids (VSGSRR) specific for Lamin C is likely to contain a target(s) of citrullination (Supplementary Fig. S3a). Hence, we constructed plasmids expressing various types of mutant Lamin C and examined the citrullination of each mutant protein. Western blotting with anti-MC antibody revealed that substitution of both 571st and 572nd arginine residues caused a significant reduction of protein citrullination (Fig. 5d). Accordingly, we raised an antibody against citrullinated Lamin C at these two arginine residues (Supplementary Fig. S3b). This antibody clearly recognized the citrullinated Lamin C in PADI4-introduced HEK293T cells as [27]

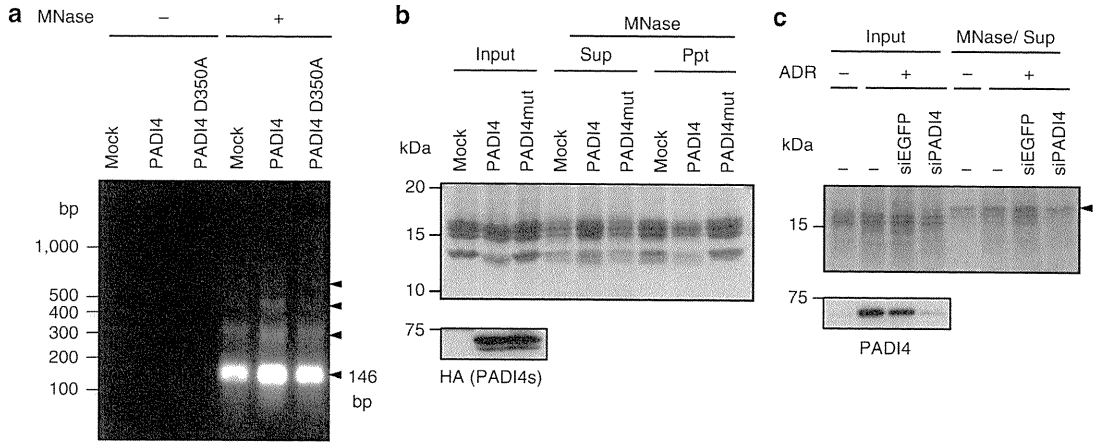

Figure 4 | Regulation of DNA cleavage by PADI4. (**a**) Chromatin was isolated from HEK293T cells transfected with PADI4 expressing plasmid. Chromatin extracted from equal numbers of cells was digested with MNase at 37 °C for 2 min. Soluble DNA released from MNase-treated chromatin were subjected to agarose gel electrophoresis. Arrow heads denote mono- and poly-nucleosomal DNAs. (**b**) Chromatin was isolated from HEK293T cells transfected with PADI4-expressing plasmid. Chromatin extracted from equal numbers of cells was digested with MNase at 37 °C for 2 min. Soluble core histones released from MNase-treated chromatin were subjected to SDS-PAGE. CBB staining for input chromatin is shown as controls. Input chromatin was subjected to immunoblotting with anti-HA antibody. (**c**) Chromatin was isolated from U-2 OS cells treated with ADR. Each siRNA was transfected 10 h before DNA damage treatment. siEGFP was used as a control. Chromatin extracted from equal numbers of cells was digested with MNase at 37 °C for 2 min. Soluble core histones released from MNase-treated chromatin were subjected to SDS-PAGE. CBB staining for input chromatin is shown as controls. Input chromatin was subjected to immunoblotting with anti-PADI4 antibody. Arrow head indicates MNase.

well as ADR-treated U-2 OS cells (Fig. 5e). In addition, immunocytochemistry revealed that the citrullinated Lamin C was localized predominantly around the fragmented nuclei in the damaged U-2 OS (Fig. 5f) and MCF7 cells (Supplementary Fig. S4a). Furthermore, cit-Lamin C expression was significantly correlated with the apoptotic cells in ADR-treated U-2 OS cells (Supplementary Fig. S4b), suggesting the involvement of citrullination of Lamin C in the nuclear fragmentation during apoptosis. Taken together, PADI4 could mediate the critical steps of apoptotic cell death through the citrullination of the core histones and Lamin C.

***Padi4*$^{-/-}$ mice exhibits apoptosis resistance.** To further investigate the physiological function of Padi4, we generated *Padi4*$^{-/-}$ mice (Supplementary Fig. S5). *Padi4*$^{-/-}$ mice were grossly normal in terms of survival, physical appearance and organ morphology. Then, we prepared messenger RNAs of thymuses from γ-ray-irradiated mice. The result of quantitative real-time PCR demonstrated that *Padi4* mRNA was significantly increased after DNA damage in wild-type mice but not in *Padi4*-deficient mice, compared with *p21*^{Waf1} as a positive control (Fig. 6a). We also detected the γ-ray-induced PADI4 expression in U-2 OS cells in a dose-dependent manner (Supplementary Fig. S6a). Immunohistochemical analysis of *in vivo* citrullination of H4R3 in *Padi4*$^{+/+}$ mice exhibited the significant signal of cit-H4R3 in thymus at 24 h after γ-ray irradiation, although cit-H4R3 was not detected in *Padi4*$^{-/-}$ mice (Fig. 6b). Concordantly, the numbers of TUNEL-positive and cleaved caspase-3-positive-cells were decreased in *Padi4*$^{-/-}$ mice (Fig. 6c,d). We also found that X-ray irradiation induced expressions of mouse *Padi4* and human *PADI4* in a p53-dependent manner (Supplementary Fig. S6b–d). Subsequently, we examined by western blotting, the level of cleaved caspase-3 in X-ray-irradiated thymus and found the significant reduction of cleaved caspase-3 in *Padi4*$^{-/-}$ mice (Fig. 6e), further supporting a critical role of Padi4 in the apoptotic process.

Frequent missense mutations of *PADI4* in cancer cell lines. To verify the biological and clinical significance of PADI4 in human carcinogenesis, we performed DNA sequencing of the *PADI4* gene in 22 breast, 21 colorectal and 37 lung cancer cell lines (Supplementary Table S1). We identified six missense mutations in six cell lines, among which the wild-type *PADI4* allele was lost in three cell lines (Supplementary Fig. S7a). As these mutations were not likely to affect the mRNA expression level (Supplementary Fig. S7b), we constructed plasmid vectors expressing either of six mutant PADI4 proteins and transfected either of these plasmids into HEK293T cells. Although T79 mutation did not affect enzymatic activity, five of six mutations lead to the remarkable decrease in enzymatic activity (Fig. 7a). Interestingly, T79 was not strictly conserved, while other five mutations were highly conserved among 14 mammalian species (Supplementary Table S2). These findings suggested the complete loss of PADI4 activity in MDA-MB-435S and SK-BR-3 cells. In concordance with this result, ectopic expression of p53 using adenovirus vector expressing p53 (Ad-p53) in MDA-MB-435S cells did not induce H4R3 citrullination, while H4R3 citrullination was observed in MDA-MB-231 cells in which wild-type PADI4 was retained (Fig. 7b). Moreover, citrullination of H4R3 was significantly associated with apoptosis induction of Ad-p53-infected MDA-MB-231 cells (Supplementary Fig. S7c), indicating a critical role of PADI4-mediated histone H4 citrullination in a p53-related pathway. Similarly, Ad-p53 infection enhanced citrullination of Lamin C only in cells in which both *PADI4* alleles are intact (Supplementary Fig. S7d). Because PADI4 was expected to function as a homodimer[23], our findings suggested that mutant PADI4 would exhibit dominant-negative activity. Although *PADI4* was mutated in LoVo cells, citrullination of Lamin C was remarkably increased in these cells. We assume that *PADI1*, *PADI2* and *PADI3* belonging to the PADI family might mediate the citrullination of Lamin C in LoVo cells because of relatively high levels of expression of these three members (Supplementary Fig. S7e).

PADI4 is a potential tumour suppressor. We examined the citrullination of H4R3 by tissue microarrays consisting of 309 NSCLC tissues (Fig. 7c). Clinicopathological analysis revealed that cit-H4R3 was associated with smaller tumour size ($P = 0.0136$ by Student's *t*-test, Table 1). We also found that 5-year survival rate in patients with cit-H4R3 expression (58.1%) was slightly longer than that in

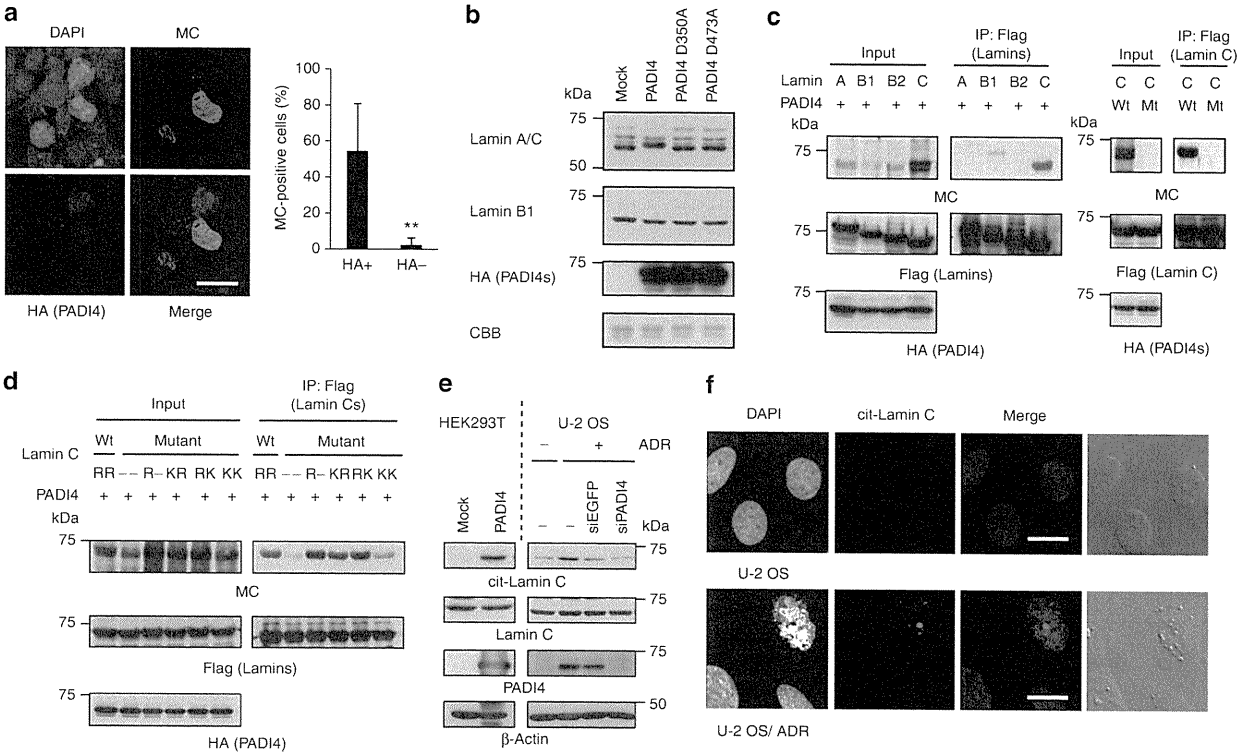

Figure 5 | Lamin C is citrullinated during nuclear fragmentation. (**a**) Representative image of HA-PADI4-transfected HEK293T cells stained with anti-modified citrulline (MC) antibody (Alexa Fluor 488) and anti-HA antibody (Aleza Fluor 594) (left panel). The proportion of MC-positive cells stratified by HA-PADI4 expression was indicated (right panel). Error bars represent s.d. ($n=9$). $^{**}P<0.01$ by Student's t-test. Scale bars, 20 μm. Cells were incubated with 5 μmol l^{-1} of A23187 for 1 h before fixation. (**b**) Western blotting for nuclear extracts from HEK293T cells transfected with wild-type PADI4, mutant PADI4 (D350A or D473A), or mock plasmid using each anti-Lamin antibody. (**c**) HEK293T cells were transfected with the indicated plasmids. Cell extracts were immunoprecipitated using anti-Flag antibody, followed by immunoblotting with anti-MC, anti-Flag, or anti-HA antibody. (**d**) HEK293T cells were transfected with the indicated plasmids. Cell extracts were immunoprecipitated using anti-Flag antibody, followed by immunoblotting with anti-MC, anti-Flag, or anti-HA antibody. (**e**) Whole-cell extracts from PADI4-transfected HEK293T cells or ADR-treated U-2 OS cells were subjected to western blotting using antibody against citrullinated Lamin C at arginine 571 and arginine 572 residues (cit-Lamin C), Lamin C, PADI4, or β-actin. Each siRNA was transfected 10 h before DNA damage treatment. siEGFP was used as a control. (**f**) Representative image of ADR-treated U-2 OS cells stained with anti-cit-Lamin C antibody (Alexa Fluor 488). Scale bars, 20 μm.

patients without cit-H4R3 expression (52.7%), although the difference was not statistically significant ($P=0.24$ by log-rank test; Fig. 7d). As many of p53 mutations lead to a prolonged half-life of p53 protein, immunohistochemistry of p53 is commonly used to detect p53 mutations in various cancers[24,25]. Interestingly, the positive p53 staining was inversely associated with cit-H4R3 staining ($P=0.0079$ by Student's t-test), indicating the regulation of chromatin modification by p53 in human carcinogenesis (Table 1).

Discussion

Accumulating evidence indicate that a combination of genetic and epigenetic alterations contribute to the development and progression of human cancers[26]. Among many genes altered in cancer tissues, the p53 gene was mutated in nearly half of all tumours[27–29]; however, the roles of p53 in histone modifications and chromatin structure have not been characterized. Here we clearly demonstrated the crucial roles of p53–PADI4 pathway in citrullination of H4R3 and Lamin C in response to DNA damage as well as in nuclear fragmentation.

A certain type or a combination of histone modifications termed as 'histone code'[30] are translated into a meaningful biological outcome such as gene expression and chromatin structure. Histone H2AX is phosphorylated at serine 139 residue (γ-H2AX) on external damage, and recruits DNA repair complex to promote chromatin remodelling[31,32]. Recently, phosphorylation of serine 14 residue in H2B, which was induced on several apoptotic stimuli including DNA damage[33], was proposed as a 'death code, but its physiological significance remains to be determined. Histone methylation, phosphorylation and acetylation are reversible processes that are regulated by histone-modifying enzymes[34]. In contrast, citrullination is a chemically stable modification, and decitrullination enzymes have not yet been discovered[35]. Therefore, histone citrullination is considered to be an irreversible cellular process. As histone H4 citrullination is associated with apoptosis of damaged cells as well as neutrophilic death triggered by NET formation, histone H4 citrullination could be defined as a functional apoptotic histone code.

Li *et al.* previously reported that PADI4 negatively regulated the $p21^{WAF1}$ expression through the interaction with p53 at a $p21^{WAF1}$ promoter region in ultraviolet-irradiated U-2 OS cells[36]. In addition, PADI4 was shown to be transactivated in various cancer tissues[37], and siPADI4 or PADI4 inhibitor (Cl-amidine) suppressed proliferation of U-2 OS cells[36], suggesting PADI4 to function as an oncogene. However, the frequent inactivating mutations of *PADI4* in cancer cell lines as well as apoptosis-resistance in *Padi4*-null mice implied the possible role of PADI4 as a tumour suppressor. This discrepancy could be partially due to the difference in the experimental conditions. We analysed the effects of PADI4 knockdown using irradiated mice or ADR-treated cells, whereas Li *et al.* analysed U-2 OS cells under the non-stress condition or after ultraviolet treatment.

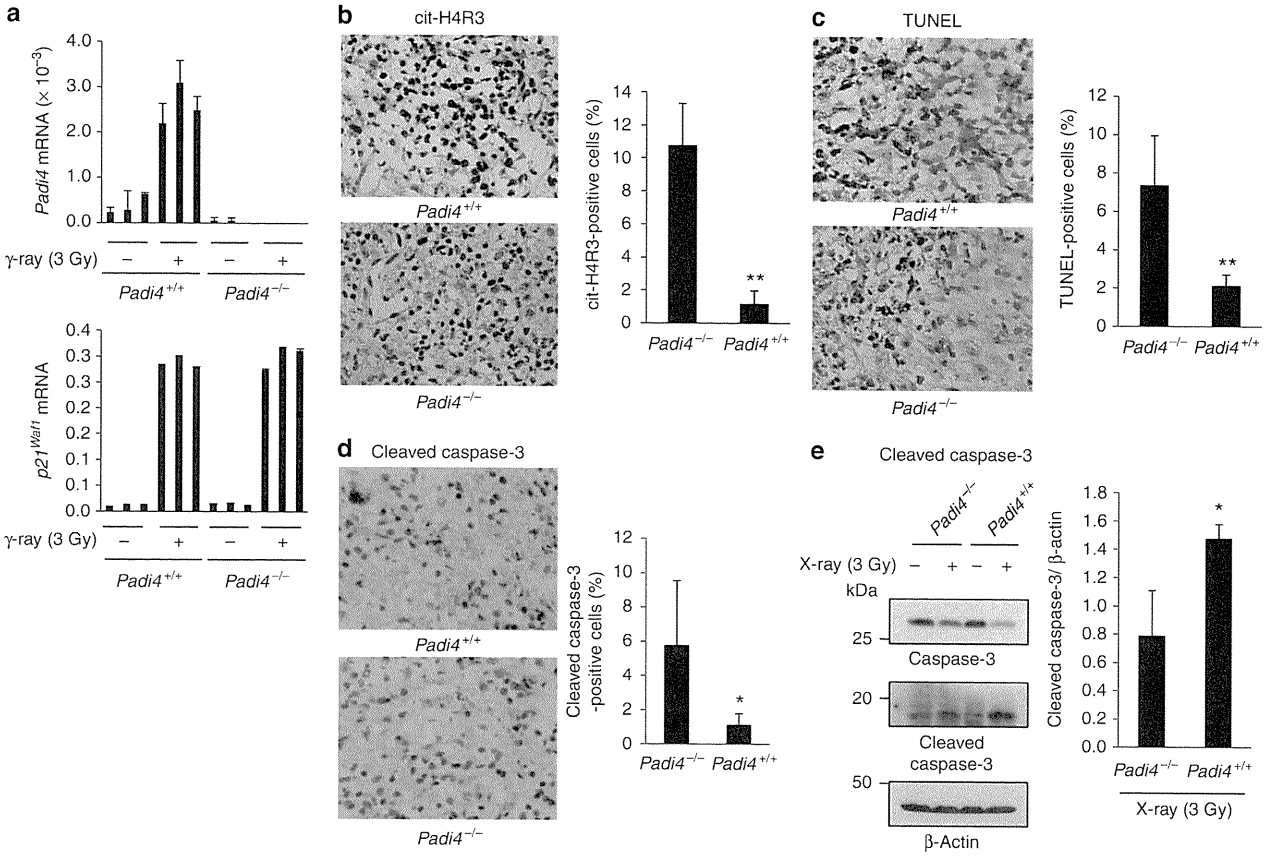

Figure 6 | The role of Padi4 in DNA damage induced apoptosis *in vivo*. (**a**) Quantitative real-time PCR analysis of *Padi4* and $p21^{Waf1}$ expression in thymuses from γ-ray-irradiated $Padi4^{-/-}$ or $Padi4^{+/+}$ mice (3 Gy). Error bars represent range ($n=2$). *Gapdh* was used for normalization of *Padi4* expression levels. Mice were sacrificed 24 h after irradiation with 3 Gy of γ-ray. (**b**) Representative images of thymus sections from γ-ray-irradiated $Padi4^{-/-}$ or $Padi4^{+/+}$ mouse 24 h after irradiation with 3 Gy of γ-ray stained for citrullinated histone H4R3 (cit-H4R3) (left panel, X40). The proportion of positive cells in $Padi4^{-/-}$ or $Padi4^{+/+}$ mouse was indicated (right panel). Error bars represent s.d. ($n=4$). $^{**}P<0.01$ by Student's *t*-test. (**c**) Representative images of TUNEL staining for thymus sections from γ-ray-irradiated $Padi4^{-/-}$ or $Padi4^{+/+}$ mouse 24 h after irradiation with 3 Gy of γ-ray (left panel, X40). The proportion of positive cells in $Padi4^{-/-}$ or $Padi4^{+/+}$ mouse was indicated (right panel). Error bars represent s.d. ($n=4$). $^{**}P<0.01$ by Student's *t*-test. (**d**) Representative images of cleaved-caspase-3 staining in thymus sections from γ-ray-irradiated $Padi4^{-/-}$ or $Padi4^{+/+}$ mouse 24 h after irradiation with 3 Gy of γ-ray (left panel, X40). The proportion of positive cells in $Padi4^{-/-}$ or $Padi4^{+/+}$ mouse was indicated (right panel). Error bars represent s.d. ($n=4$). $^{*}P<0.05$ by Student's *t*-test. (**e**) Whole-cell extracts of thymus from X-ray-irradiated $Padi4^{-/-}$ or $Padi4^{+/+}$ mice were subjected to immunoblotting with anti-cleaved caspase-3, anti-caspase-3 or anti-β-actin antibody (left panel). Mice were sacrificed 48 h after irradiation with 3 Gy of X-ray. The ratio between cleaved caspase-3 and β-actin from independent samples ($n=4$ for $Padi4^{-/-}$ mice and $n=2$ for $Padi4^{+/+}$ mice) was indicated (right panel). $^{*}P<0.05$ by Student's *t*-test.

Although ADR- or γ-ray-treatment remarkably increased PADI4 expression, ultraviolet-treatment did not induce *PADI4* expression in U-2 OS cells (Supplementary Fig. S8a). In addition, expression levels of $p21^{Waf1}$ in thymus in the $Padi4^{+/+}$ and $Padi4^{-/-}$ mice after γ-ray irradiation were not significantly different (Fig. 6a). Similarly, siPADI4 treatment did not affect the expression of p53-target genes including $p21^{WAF1}$ in ADR-treated U-2 OS cells (Supplementary Fig. S8b). Moreover, siPADI4-treated U373MG cells exhibited resistance to p53-induced apoptosis (Supplementary Fig. S8c). In fact, we observed the citrullination of histone H4R3 in 51.5% of lung cancer tissues, suggesting the activation of PADI4 in a large proportion of cancer tissues, as suggested in the previous report[37]. However, cancer tissues are persistently exposed to oxidative stress compared with adjacent normal tissues[38,39], activation of PADI4 would be related with cellular stress condition. Taken together, we assume that PADI4 could predominantly function as a tumour suppressor that mediates the apoptotic process of damaged cells.

Although the molecular mechanism of how PADI4 increases DNA accessibility was not fully elucidated, loss of positive charge by citrullination was shown to induce conformational changes of histone H4 N terminal[40]. DNA–histone interaction is charge-dependent, and changes in the charge of the histone tails are considered to weaken histone-DNA interaction[41]. Moreover, we found that the interaction between core histones and nucleophosmin was inhibited by citrullination (Supplementary Fig. S8d). Any or all of these changes can affect the structure and folding of individual nucleosome that could lead to a more open and permissive chromatin environment. The role of PADI4 in chromatin remodelling was shown in the previous papers[42,43]. We also reported that DNA damage induced PADI4 expression and the citrullination of various proteins in our previous study[10]. To our knowledge, this is the first report demonstrating the important role of histone H4R3 citrullination in human carcinogenesis and the p53-mediated apoptotic pathway.

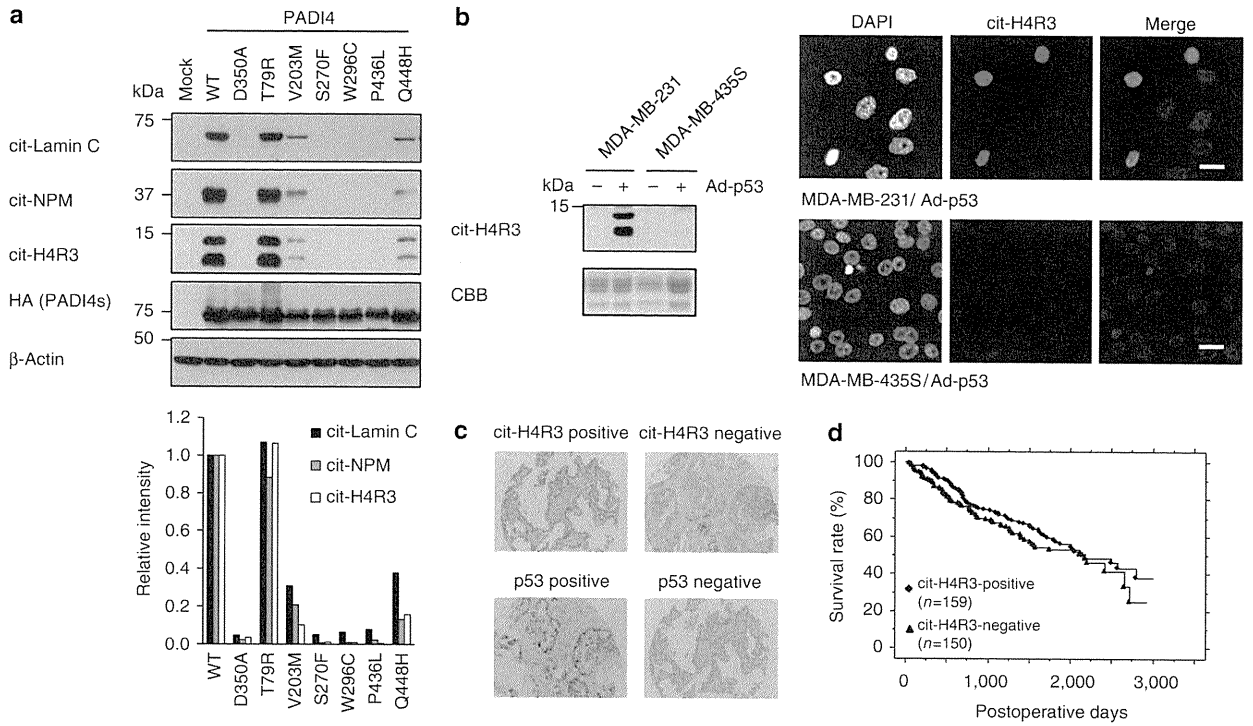

Figure 7 | Involvement of PADI4 in carcinogenesis. (**a**) Whole-cell extracts from HEK293T cells transfected with wild-type or mutant PADI4 were subjected to western blotting using anti-citrullinated Lamin C (cit-Lamin C), anti-citrullinated nucleophosmin (cit-NPM), anti-citrullinated histone H4R3 (cit-H4R3), anti-HA, or anti-β-actin antibody (upper panel). For quantification, band intensities were normalized to the signal in cells transfected with wild-type PADI4 (lower panel). (**b**) MDA-MB-231 and MDA-MB-435S cells were infected with adenovirus vector expressing p53 (Ad-p53). Histones were subjected to western blotting using anti-cit-H4R3 (left panel). Representative images of Ad-p53-infected cells stained for cit-H4R3 is shown in right panel. Scale bars, 20 μm. (**c**) cit-H4R3 or p53 expression in NSCLC tissues (magnification X10). (**d**) Kaplan-Meier analysis of survival in patients with NSCLC according to the expression of cit-H4R3 ($P = 0.24$, log-rank test).

Methods

Cell culture and transfections. Cell lines were purchased from American Type Culture Collection, Lonza Biologics, or Japanese Collection of Research Bioresources. Cells were transfected with plasmids using FuGENE6 (Roche). Replication-deficient recombinant viruses Ad-p53 or Ad-LacZ, expressing p53 or LacZ, respectively, were generated and purified, as described previously[5]. siRNA oligonucleotides, commercially synthesized by Sigma Genosys, were transfected with Lipofectamine RNAiMAX reagent or Lipofectamine 2000 reagent (Invitrogen). Sequences of oligonucleotides are shown in Supplementary Table S3. For treatment with calcium ionophore, cells were incubated with 5 μM of A23187 (Calbiochem) for 1 h at 37 °C.

Plasmid construction. Complementary DNA fragments of Lamin A, Lamin B1, Lamin B2 and Lamin C were amplified and cloned into pCAGGS vector. PADI4 expression plasmids were previously described[10]. Plasmids expressing mutant PADI4 or Lamin C were generated using the inverse PCR methods or by using the reverse primer containing point mutation at either or both of arginine 571 and 572 residues, respectively. The primer sequences for cloning and mutagenesis are shown in Supplementary Table S3.

Knockout mice. We amplified a 5,837 bp fragment containing exon 1 and exon 2 of *Padi4* using C57BL/6 genomic DNA as a template. The targeting vector was designed to replace exon 1 and 2, including the transcription initiation site, by mouse PGK-1 promoter and the neomycin-resistance gene (Supplementary Fig. S5a). We introduced the linearized targeting vector by electroporation into embryonic stem cells, and identified two independent targeted 129S1 embryonic stem cell clones by Southern blot analysis. We generated chimeric males by the aggregation method and crossed them with C57BL/6 females, and verified germline transmission by Southern blot analysis (Supplementary Fig. S5b,c). All *Padi4*$^{-/-}$ mice used in this study had been backcrossed for ten generations into the C57BL/6 background. We used RT–PCR to determine the presence of the *Padi4* transcript (Supplementary Fig. S5d). p53-deficient mice were provided from RIKEN BioResource Center (Ibaragi, Japan)[44]. Genotypes were confirmed by PCR analysis. The primer sequences are indicated in Supplementary Table S3. All mice were maintained under specific pathogen-free conditions and were handled in accordance with the Guidelines for Animal Experiments of the Institute of Medical Science (University of Tokyo, Tokyo, Japan).

DNA damaging treatment. For treatment with genotoxic stress, cells were continuously incubated with 2 μg ml^{-1} ADR for 2 h, γ-irradiated using a Cs-137 source (Gamma cell-40, Atomic energy of Canada), ultraviolet-irradiated using an ultraviolet cross-linker (XL-1500, Spectronics corporation), or X-irradiated using an X-ray irradiation system (MBR-1520R-3, Hitachi). Mice were also γ-irradiated using a Cs-137 source (Gamma cell-40, Nordion) or X-irradiated using an X-ray irradiation system (MBR-1520R-3, Hitachi).

Quantitative real-time PCR. Peripheral blood mononuclear cells were obtained by separating blood cells in a Ficoll gradient (Amersham). Peripheral blood mononuclear cells were incubated with phytohaemagglutinin for 72 h and exposed to an X-ray irradiation. Total RNA was isolated from mouse tissue or human cells using RNeasy spin column kits (Qiagen) according to the manufacturer's instruction. Blood RNA of irradiated mice was prepared using Mouse RiboPure-Blood RNA Isolation Kit (Ambion). Complementary DNAs were synthesized with the SuperScript Preamplification System (Invitrogen). Quantitative real-time PCR was conducted using the SYBR Green I Master on a LightCycler 480 (Roche). The primer sequences are indicated in Supplementary Table S3.

Immunoprecipitation. Cell extracts from HEK293T cells transfected with plasmids encoding Flag-Lamins and/or HA-PADI4s were prepared by adding HBST buffer (10 mM HEPES at pH 7.4, 150 mM NaCl and 0.5% TritonX-100). Extracts were precleared by incubation with protein G-Sepharose 4B (Zymed) and mouse IgG at 4 °C for 1 h. Precleared cell extracts were then incubated with anti-Flag affinity gel (Sigma) at 4 °C for 2 h. The beads were washed 4 times with 1 ml of ice-cold HBST buffer, and immunoprecipitated proteins were released from the beads by boiling in sample buffer for 2 min.

Western blotting. To prepare whole-cell extracts, cells or tissues were lysed in chilled HBST buffer for 30 min on ice and centrifuged at 16,000*g* for 15 min. Histones were purified in acidic condition as previously described[45]. Samples were subjected to SDS–PAGE and immunoblotting using standard procedures. To detect citrullinated proteins, blots of deiminated proteins were treated with medium for chemical modification at 37 °C for 3 h, and, then, modified citrulline residues were detected with an anti-modified citrulline antibody (anti-MC antibody, Upstate). Bands were quantified by the Image J software.[31]

Table 1 | Association between citrullinated H4R3-positivity and clinicopathological parameters in NSCLC patients.

	Total	cit-H4R3		*P* value
	n=309	Positive	Negative	Positive versus negative
		n=159	*n*=150	
Gender				
Male	214	100	114	0.0138**
Female	95	59	36	
Age (years)				
<65	135	67	68	NS (0.6463)
≧65	174	92	82	
Histological type				
ADC	192	110	82	0.0099**
SCC	82	35	47	
Others	35	14	21	
Smoking status				
Never	90	60	30	0.0007**
Smoker	219	99	120	
pT factor				
T1	132	80	52	0.0136**
T2+T3	177	79	98	
pN factor				
N0	204	104	100	NS (0.9044)
N1+N2	105	55	50	
p53				
Positive	130	55	75	0.0079**
Negative	179	104	75	

Abbreviations: ADC, adenocarcinama; NS, no significance; SCC, squamous-cell carcinoma; Others, large-cell carcinoma plus adenosquamous-cell carcinoma.
**$P<0.05$ (Fisher's exact test).

Antibodies. To develop an antibody against Cit571-572 Lamin C, a Lamin C peptide (LHHHHVSGSCitCit) was chemically synthesized and used to immunize rabbits. The positive antisera were further purified by immune-affinity purification using a Lamin C Cit571-572 peptide. Anti-citrullinated nucleophosmin (NPM) antibody was prepared as previously described[10]. Polyclonal anti-MC antibody (17-347) and anti-citrullinated arginine 3 of histone H4 antibody (07-596) were purchased from Upstate. Anti-β-actin monoclonal antibody (A5441) and Anti-Flag monoclonal (F3165) and polyclonal (F7425) antibodies were purchased from Sigma. Anti-p53 monoclonal antibody (OP140) and anti-Lamin B antibody (NA12) were purchased from Calbiochem. Anti-HA monoclonal (sc-7392) and polyclonal (sc-805) antibodies were purchased from Santa Cruz Biotechnology. Anti-HA rat monoclonal antibody (3F10) was purchased from Roche. Anti-6×His monoclonal antibody (631212) was purchased from Clontech. Anti-PADI4 polyclonal antibody (ab50332), anti-citrullinated histone H3 antibody (ab5103) and anti-mono methyl histone H4 antibody (ab17339) were purchased from Abcam. Anti-Lamin A/C antibody (#2032 or #4777), anti-caspase-3 antibody (#9662) and anti-cleaved caspase-3 (#9661) were purchased from Cell signaling. List of antibodies and the concentrations used are shown in Supplementary Table S4.

***In vitro* citrullination assay**. Recombinant histone proteins were purchased from Millipore. Glutathione *S*-transferase (GST) fusion PADI4 and NPM1 proteins were generated as previously described[10]. His-tagged proteins were generated by cloning of their coding sequences into pET21a or pET28a vector (Novagen). Proteins were expressed in *Escherichia coli* and purified on Ni-NTA agarose (Qiagen) by standard methods. Deimination reactions were carried out as previously described[10].

GST pull-down assay. Core histones were purified from HEK293T cells using Histone Purification Kit (Active motif). GST-NPM (1 μg) and core histones (1 μg) were separately incubated with PADI4 (1 μg) or PADI4-D350A (1 μg) for 1 h at 37 °C with 1 mM of CaCl2. PADI4-treated NPM1 and histones were mixed and stored on ice for 1 h. The mixture was incubated at 4 °C for 2 h with 20 μl of a glutathione–Sepharose 4B bead suspension (Amersham Pharmacia). After the beads were washed extensively, proteins were eluted from the beads by incubation with SDS sample buffer, separated by SDS–PAGE, and visualized by silver staining.

Immunocytochemistry. Immunocytochemistry was performed as previously described[10]. Before incubating with anti-MC antibody, cells were treated with medium for chemically modifying citrulline residues at 37 °C for 3 h. For co-staining of TUNEL and citrullinated proteins, cells were immunostained followed by TUNEL reaction for 1 h at 37 °C using the kit (In Situ Cell Death Detection Kit, Fluorescein, Roche). Quantification was performed by counting around 100 cells from more than 4 independent fields.

Immunohistochemistry. Frozen sections of mouse thymus were used for immunohistochemistry and TUNEL staining. Immunohistochemistry was performed using the immunohistochemistry EnVision (Dako) method. TUNEL staining was performed using Apoptosis in situ Detection Kit (Wako) according to the manufacturer's instruction. Tissue microarrays were constructed in our laboratory, and staining and statistical analysis were performed as previously described[46].

Mutation analysis. Genomic DNA was purified from 80 cancer cell lines by standard protocol[8]. The list of cell lines is shown in Supplementary Table S1. 16 coding exons of the *PADI4* gene were amplified, purified and sequenced. The sequences of primers used in this analysis are indicated in Supplementary Table S3.

Chromatin fractionation. S1, S2 and P chromatin fractions from HEK293T cell nuclei were prepared according to previously described procedures[47] with minor modifications. HEK293T cells were transfected with PADI4-expressing plasmid. The collected cells were incubated in cell homogenization buffer (10 mM Tris at pH 8.0, 10 mM $MgCl_2$, 0.5% NP40 and 1 mM DTT) on ice for 10 min. The nuclear pellet was obtained by centrifugation and resuspended in MNase digestion buffer (15 mM Tris pH 7.4, 15 mM NaCl, 60 mM KCl, 0.25 M sucrose, 1 mM $CaCl_2$). The pellet was then treated with MNase (New England Biolabs) for 2 min at 37 °C. The solution was centrifuged to obtain the supernatant (S1). The pellet was resuspended in 0.1 mM EDTA, incubated at 4 °C for 30 min, and centrifugated to obtain the chromatin fraction (P) and supernatant (S2). The proteins contained in each fraction were separated by 15% SDS–PAGE and detected by western blotting.

MNase assay. The nuclear pellet (Input) was treated with MNase as shown above. The reaction was terminated by adding the stop solution (0.5 mM EGTA, 25 mM EDTA). After centrifugation at 14,000*g* for 5 min, DNA was extracted from the aqueous phase and analysed on agarose gel. Histone proteins collected from the aqueous phase (Sup) and pellet (Ppt) were separated by SDS–PAGE.

Cell death assay. Cells were infected with 20 multiplicity of infection (MOI) of Ad-p53 at 7 h after transfection of siRNA oligonucleotide. 60 h after infection cells were incubated with TUNEL reaction mixture for 1 h at 37 °C using the kit (In Situ Cell Death Detection Kit, Fluorescein, Roche). Apoptotic cells were quantified by fluorescence-activated cell sorting analysis.

References

1. Levine, A. J., Hu, W. & Feng, Z. The P53 pathway: what questions remain to be explored? *Cell Death and Differ.* **13,** 1027–1036 (2006).
2. Vogelstein, B., Lane, D. & Levine, A. J. Surfing the p53 network. *Nature* **408,** 307–310 (2000).
3. Lane, D. P. Cancer. p53, guardian of the genome. *Nature* **358,** 15–16 (1992).
4. Nakamura, Y. Isolation of p53-target genes and their functional analysis. *Cancer Sci.* **95,** 7–11 (2004).
5. Oda, K. *et al.* p53AIP1, a potential mediator of p53-dependent apoptosis, and its regulation by Ser-46-phosphorylated p53. *Cell* **102,** 849–862 (2000).
6. Tanaka, H. *et al.* A ribonucleotide reductase gene involved in a p53-dependent cell-cycle checkpoint for DNA damage. *Nature* **404,** 42–49 (2000).
7. Tanikawa, C., Matsuda, K., Fukuda, S., Nakamura, Y. & Arakawa, H. p53RDL1 regulates p53-dependent apoptosis. *Nat. Cell Biol.* **5,** 216–223 (2003).
8. Tanikawa, C. *et al.* XEDAR as a putative colorectal tumor suppressor that mediates p53-regulated anoikis pathway. *Oncogene* **28,** 3081–3092 (2009).
9. Tanikawa, C., Ri, C., Kumar, V., Nakamura, Y. & Matsuda, K. Crosstalk of EDA-A2/XEDAR in the p53 signaling pathway. *Mol. Cancer Res.* **8,** 855–863 (2010).
10. Tanikawa, C. *et al.* Regulation of protein citrullination through p53/PAD14 network in DNA damage response. *Cancer Res.* **69,** 8761–8769 (2009).
11. Nakashima, K., Hagiwara, T. & Yamada, M. Nuclear localization of peptidylarginine deiminase V and histone deimination in granulocytes. *J. Biol. Chem.* **277,** 49562–49568 (2002).
12. Neeli, I., Khan, S. N. & Radic, M. Histone deimination as a response to inflammatory stimuli in neutrophils. *J. Immunol.* **180,** 1895–1902 (2008).
13. Wang, Y. *et al.* Histone hypercitrullination mediates chromatin decondensation and neutrophil extracellular trap formation. *J. Cell Biol.* **184,** 205–213 (2009).
14. de Seze, J. *et al.* IgG reactivity against citrullinated myelin basic protein in multiple sclerosis. *J. Neuroimmunol.* **117,** 149–155 (2001).
15. Schellekens, G. A. *et al.* The diagnostic properties of rheumatoid arthritis antibodies recognizing a cyclic citrullinated peptide. *Arthritis Rheum.* **43,** 155–163 (2000).
16. Goldbach-Mansky, R. *et al.* Rheumatoid arthritis associated autoantibodies in patients with synovitis of recent onset. *Arthritis Res.* **2,** 236–243 (2000).

17. van Boekel, M. A., Vossenaar, E. R., van den Hoogen, F. H. & van Venrooij, W. J. Autoantibody systems in rheumatoid arthritis: specificity, sensitivity and diagnostic value. *Arthritis Res.* **4,** 87–93 (2002).
18. Suzuki, A. *et al.* Functional haplotypes of PADI4, encoding citrullinating enzyme peptidylarginine deiminase 4, are associated with rheumatoid arthritis. *Nat. Genet.* **34,** 395–402 (2003).
19. Wang, Y. *et al.* Human PAD4 regulates histone arginine methylation levels via demethylimination. *Science* **306,** 279–283 (2004).
20. Cuthbert, G. L. *et al.* Histone deimination antagonizes arginine methylation. *Cell* **118,** 545–553 (2004).
21. Martic, G. *et al.* Parathymosin affects the binding of linker histone H1 to nucleosomes and remodels chromatin structure. *J. Biol. Chem.* **280,** 16143–16150 (2005).
22. Li, P. *et al.* PAD4 is essential for antibacterial innate immunity mediated by neutrophil extracellular traps. *J. Exp. Med.* **207,** 1853–1862 (2010).
23. Arita, K. *et al.* Structural basis for Ca(2+)-induced activation of human PAD4. *Nat. Struct. Mol. Biol.* **11,** 777–783 (2004).
24. Top, B. *et al.* Comparative analysis of p53 gene mutations and protein accumulation in human non-small-cell lung cancer. *Int. J. Cancer* **64,** 83–91 (1995).
25. Bodner, S. M. *et al.* Expression of mutant p53 proteins in lung cancer correlates with the class of p53 gene mutation. *Oncogene* **7,** 743–749 (1992).
26. Jones, P. A. & Baylin, S. B. The epigenomics of cancer. *Cell* **128,** 683–692 (2007).
27. Hollstein, M. *et al.* Database of p53 gene somatic mutations in human tumors and cell lines. *Nucleic Acids Res.* **22,** 3551–3555 (1994).
28. Soussi, T. *et al.* Meta-analysis of the p53 mutation database for mutant p53 biological activity reveals a methodologic bias in mutation detection. *Clin. Cancer Res.* **12,** 62–69 (2006).
29. Beroud, C. & Soussi, T. The UMD-p53 database: new mutations and analysis tools. *Hum. Mutat.* **21,** 176–181 (2003).
30. Jenuwein, T. & Allis, C. D. Translating the histone code. *Science* **293,** 1074–80 (2001).
31. Celeste, A. *et al.* H2AX haploinsufficiency modifies genomic stability and tumor susceptibility. *Cell* **114,** 371–383 (2003).
32. Bassing, C. H. *et al.* Histone H2AX: a dosage-dependent suppressor of oncogenic translocations and tumors. *Cell* **114,** 359–370 (2003).
33. Cheung, W. L. *et al.* Apoptotic phosphorylation of histone H2B is mediated by mammalian sterile twenty kinase. *Cell* **113,** 507–517 (2003).
34. Kouzarides, T. Chromatin modifications and their function. *Cell* **128,** 693–705 (2007).
35. Gyorgy, B., Toth, E., Tarcsa, E., Falus, A. & Buzas, E. I. Citrullination: a posttranslational modification in health and disease. *Int. J. Biochem. Cell Biol.* **38,** 1662–1677 (2006).
36. Li, P. *et al.* Regulation of p53 target gene expression by peptidylarginine deiminase 4. *Mol. Cell. Biol.* **28,** 4745–4758 (2008).
37. Chang, X. *et al.* Increased PADI4 expression in blood and tissues of patients with malignant tumors. *BMC Cancer* **9,** 40 (2009).
38. Brown, N. S. & Bicknell, R. Hypoxia and oxidative stress in breast cancer. Oxidative stress: its effects on the growth, metastatic potential and response to therapy of breast cancer. *Breast Cancer Res.* **3,** 323–327 (2001).
39. Toyokuni, S., Okamoto, K., Yodoi, J. & Hiai, H. Persistent oxidative stress in cancer. *FEBS Lett.* **358,** 1–3 (1995).
40. Arita, K. *et al.* Structural basis for histone N-terminal recognition by human peptidylarginine deiminase 4. *Proc. Natl Acad. Sci. USA* **103,** 5291–5296 (2006).
41. Allfrey, V. G. Structural modifications of histones and their possible role in the regulation of ribonucleic acid synthesis. *Proc. Can. Cancer Conf.* **6,** 313–335 (1966).
42. Denis, H. *et al.* Functional connection between deimination and deacetylation of histones. *Mol. Cell Biol.* **29,** 4982–4993 (2009).
43. Li, P. *et al.* Coordination of PAD4 and HDAC2 in the regulation of p53-target gene expression. *Oncogene* **29,** 3153–3162 (2010).
44. Tsukada, T. *et al.* Enhanced proliferative potential in culture of cells from p53-deficient mice. *Oncogene* **8,** 3313–3322 (1993).
45. Shechter, D., Dormann, H. L., Allis, C. D. & Hake, S. B. Extraction, purification and analysis of histones. *Nat. Protoc.* **2,** 1445–1457 (2007).
46. Kato, T. *et al.* Activation of placenta-specific transcription factor distal-less homeobox 5 predicts clinical outcome in primary lung cancer patients. *Clin. Cancer Res.* **14,** 2363–2370 (2008).
47. Kashiwagi, K., Nimura, K., Ura, K. & Kaneda, Y. DNA methyltransferase 3b preferentially associates with condensed chromatin. *Nucleic Acids Res.* **39,** 874–888 (2011).

Acknowledgements

We thank H. Fujiwara for technical assistance. We thank Dr Nobuaki Yoshida and Dr. Toyomasa Katagiri for helpful discussion. This work was supported partially by grant from Japan Society for the Promotion of Science and Ministry of Education, Culture, Sports, Science and Technology of Japan to K.M. and C.T.; grant from Shiseido to C.T.; and Grant-in-Aid from the Tokyo Biochemical Research Foundation to K.M.

Author contributions

C.T., Y.N. and K.M. conceived the project and planned experiments and analyses, which were performed by C.T., M.E. conducted the mutation analysis. K.U. conducted mass analysis. A.S. and K.Y. provided the *Padi4*$^{-/-}$ mice. K.Mas., E.T. and Y.D. conducted tissue microarray analysis. C.T. summarized the whole results. C.T., K.M. and Y.N. wrote the manuscript.

Additional information

Supplementary Information accompanies this paper at http://www.nature.com/naturecommunications

Competing financial interests: The authors declare no competing financial interests.

Reprints and permission information is available online at http://npg.nature.com/reprintsandpermissions/

How to cite this article: Tanikawa, C. *et al.* Regulation of histone modification and chromatin structure by the p53–PADI4 pathway. *Nat. Commun.* 3:676 doi: 10.1038/ncomms1676 (2012).

Toyama *et al. Proteome Science* 2011, **9**:18
http://www.proteomesci.com/content/9/1/18

PROTEOME SCIENCE

RESEARCH Open Access

Deglycosylation and label-free quantitative LC-MALDI MS applied to efficient serum biomarker discovery of lung cancer

Atsuhiko Toyama[1,2,5], Hidewaki Nakagawa[2], Koichi Matsuda[1,3], Nobuhisa Ishikawa[4], Nobuoki Kohno[4], Yataro Daigo[1,3], Taka-Aki Sato[5], Yusuke Nakamura[3] and Koji Ueda[2*]

Abstract

Background: Serum is an ideal source of biomarker discovery and proteomic profiling studies are continuously pursued on serum samples. However, serum is featured by high level of protein glycosylations that often cause ionization suppression and confound accurate quantification analysis by mass spectrometry. Here we investigated the effect of N-glycan and sialic acid removal from serum proteins on the performance of label-free quantification results.

Results: Serum tryptic digests with or without deglycosylation treatment were analyzed by LC-MALDI MS and quantitatively compared on the Expressionist Refiner MS module. As a result, 345 out of 2,984 peaks (11.6%) showed the specific detection or the significantly improved intensities in deglycosylated serum samples ($P < 0.01$). We then applied this deglycosylation-based sample preparation to the identification of lung cancer biomarkers. In comparison between 10 healthy controls and 20 lung cancer patients, 40 peptides were identified to be differentially presented ($P < 0.01$). Their quantitative accuracies were further verified by multiple reaction monitoring. The result showed that deglycosylation was needed for the identification of some unique candidates, including previously unreported O-linked glycopeptide of complement component C9.

Conclusions: We demonstrated here that sample deglycosylation improves the quantitative performance of shotgun proteomics, which can be effectively applied to any samples with high glycoprotein contents.

Background

Since analyses of the serum proteome hold great promise for non-invasive detection of cancers and other diseases, various techniques for quantitative proteomic profiling have been developed to identify novel protein biomarkers [1,2]. These include labeling methods using stable isotopes such as ICAT (Isotope-coded affinity tags) [3], ^{13}CNBS (2-nitrobenzenesulfenyl) [4], SILAC (Stable isotope labeling with amino acids in cell culture) [5] and iTRAQ (Isobaric tags for relative and absolute quantification) [6]. Control and test samples are labeled with reagents with different isotopic composition of $^{12/13}$C, $^{14/15}$N and/or $^{16/18}$O, and detected simultaneously by mass spectrometry so that the intensities of isotopically resolved peak-pairs (or peak groups) represent the quantitative ratio of control and test samples. Although the precision of quantification is very high (typically 10% relative standard deviation) [7] because of the identical separation and detection, isotopic labeling limits the number of samples to be directly compared, which makes it unsuitable for analysis of a large number of clinical samples needed for biomarker discoveries. In contrast, label-free quantification methods deal with independently-acquired mass spectrometry data from essentially unlimited number of samples. Quantification based on ion intensities (extracted ion chromatograms) is known to have at least three orders of linear dynamic range [8,9], and can potentially cover wide proteome in complex samples such as serum. It is advantageous that label-free systems do not involve sample mixing prior to detection because target proteins that are only presented in test samples are effectively diluted by mixing with

* Correspondence: k-ueda@riken.jp
[2]Laboratory for Biomarker Development, Center for Genomic Medicine, RIKEN, Tsurumiku-Suehirocho1-7-22, Yokohama, Japan
Full list of author information is available at the end of the article

control samples, rendering them more difficult to detect. Therefore, label-free quantification has emerged as an alternative approach for biomarker discovery, which requires sufficient sample sizes to overcome individual variability in clinical samples and technical bias in sample preparation and analysis batch [10].

High content of glycoproteins is another feature of serum that should be considered when performing quantitative proteomic analysis. Recent advances in glycoproteomic analysis using mass spectrometry have made it possible to exhaustively identify N-linked glycopeptides and their glycosylation sites [11,12]. These techniques involve enrichment of glycopeptides followed by enzymatic cleavage of N-glycans in order for efficient mass spectrometric analysis. Deglycosylation can be coupled with the incorporation of ^{18}O stable isotope resulting in +3 Da mass shift of asparagine residues, which allows deterministic identification of glycosylation sites [13]. As these studies indicated, most of serum proteins are heavily glycosylated, however, potential effect of glycopeptides on ionization suppression of co-existing peptides had been overlooked. Glycopeptides carry large, hydrophilic carbohydrate moieties, which can cause substantial ionization suppression [14], hampering precise quantification particularly at low-concentration range.

To elucidate the extent to which the ionization of peptides is interfered by glycopeptides, the first part of this study describes the changes caused by serum deglycosylation in the MS peak profiles obtained by label-free shotgun proteomic analysis. Having shown the utility of deglycosylation, we next applied this principle to the biomarker screening of lung cancer. Because of the vast number of incidence and high mortality rate, lung cancer is considered to be one of the highest priorities for biomarker development. Using the serum samples of 10 healthy control, 10 early-stage (Stage I-II) cases and 10 advanced stage (Stages IIIb-IV) cases, we conducted a study that uniquely combined sample deglycosylation, label-free MALDI and multiple reaction monitoring (MRM) mass spectrometry [15] and verified the result by western blotting. Taken together, we show herein that enzymatic removal of carbohydrate moieties results in recognizable improvement in the data quality of shotgun proteomics in terms of sensitivity and reproducibility, which should facilitate quantitative analysis of glycoprotein-rich samples.

Results

Quantitative MS analysis of deglycosylated serum

In order to examine the effect of deglycosylation on data content and quality, tryptic digest of serum proteins was prepared with or without the removal of N-glycans and sialic acids (n = 6), and analyzed on the LC-MALDI label-free quantification platform as summarized in Figure 1. Figure 2 shows the 2-dimensional MS signal intensity maps after data processing by Expressionist Refiner MS (Genedata). In total, 27,357 single peaks were detected, comprising 4,444 groups of peaks each representing unique peptide species (termed "peak clusters"). Examples of the differences in the peak profile between deglycosylated and untreated samples are illustrated in the 2D map. The broken box in Figure 2a shows emergence of prominent peaks, and the expanded views in Figure 2c and 2d (arrows) illustrate the loss of intact glycopeptide peaks. The peak clusters subjected to comparative analysis were selected by eliminating peaks that were not presented in all of the 6 replicate runs. This filtering was performed separately for deglycosylated and untreated samples, yielding 2,984 and 2,610 peak clusters, respectively. Deglycosylation thus resulted in 14.3% increase in the number of reproducibly detectable peaks. The signal intensities of these peak profiles were then directly compared by t-test as summarized in the volcano plot (Figure 3). 221 peak clusters displayed altered intensities, of which 188 were higher in deglycosylated samples and 33 peak clusters vice versa ($P < 0.01$). Present/absent search revealed that 157 peak clusters were found specifically in deglycosylated samples (Figure S-1, Additional File 1). Combined, 345 of 2,984 peak clusters (11.6%) detected in deglycosylated samples were enhanced by deglycosylation, as opposed to 33 of 2,610 peak clusters (1.3%) in untreated serum.

The composition of the peak profiles was analyzed by exhaustive MS/MS analysis, resulting in 1,735 peptide identifications, including 153 originally-glycosylated peptides that were identified with ^{18}O-incorporated N-glycosylation sites (Table S-2, Additional File 1). By matching the peptide IDs to the statistical analysis, we found that 97 of 345 peak clusters overrepresented in deglycosylated serum were originally-glycosylated peptides. These peak clusters emerged as the product of deglycosylation and accounted for most of the major fold-changes in the volcano plot as indicated with squares in Figure 3. The remaining 248 peak clusters, as well as the 33 peak clusters that diminished by deglycosylation, were non-glycopeptides. There were no apparent features common to these peptides. Rather, signal intensities were affected by the local peptide composition, such that alleviation of suppressive analytes led to signal enhancement and emergence of competing analytes led to diminished signal. The result shown here, that the number of enhanced peaks was by far greater than those that diminished, suggest that the ionization suppression effect exerted by intact glycopeptides was more extensive than the deglycosylated counterpart.

To investigate whether deglycosylation had any effect on the quality of quantitative data, reproducibility of six

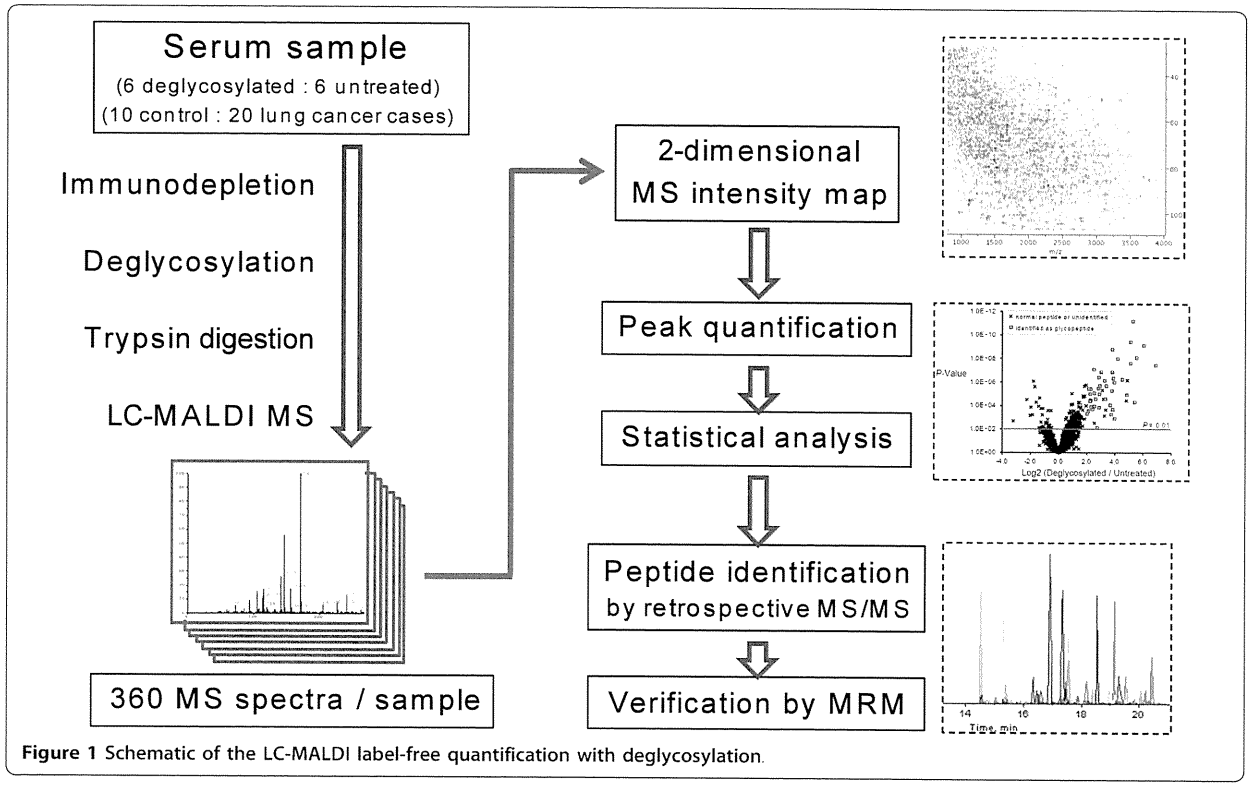

Figure 1 Schematic of the LC-MALDI label-free quantification with deglycosylation.

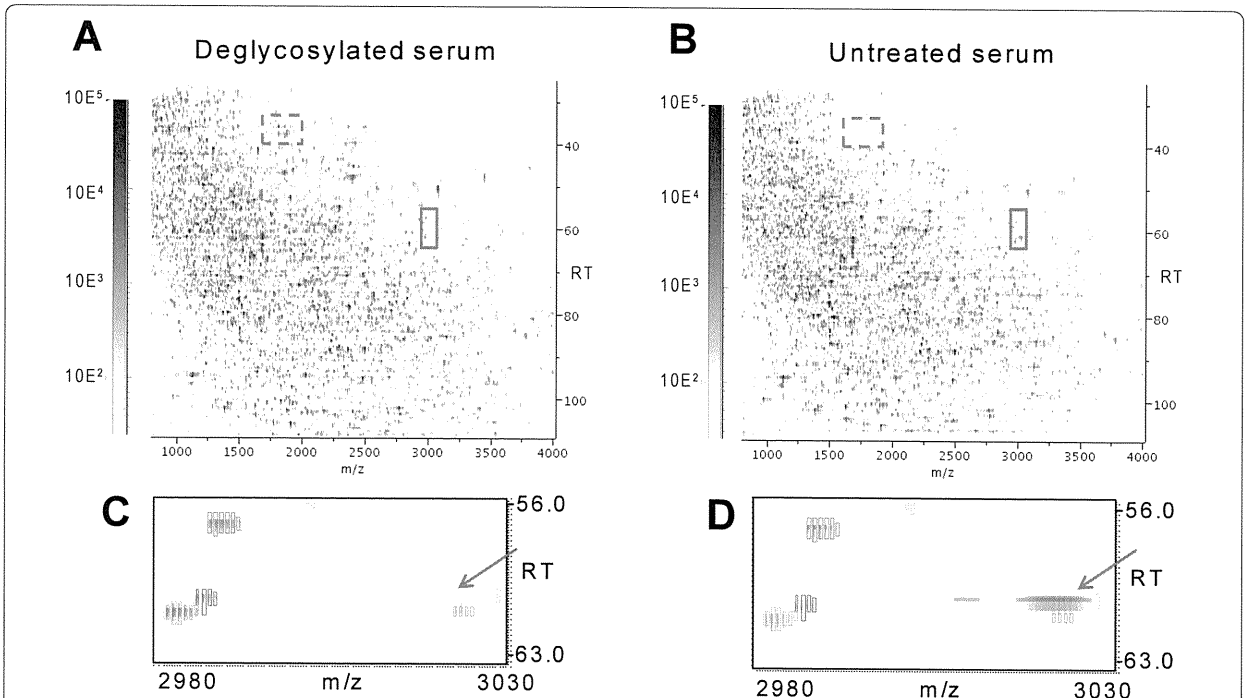

Figure 2 Representative 2-dimesional signal intensity maps visualizing the peptide profiles of (A) tryptic digest of deglycosylated serum, and (B) untreated serum, within the range of m/z 800-4000, and 25-110 minutes of retention time. An example of obvious peak appearance in deglycosylated serum is indicated by broken boxes. (C) and (D) display the expanded views of the closed box in deglycosylated sample and untreated sample, respectively. The rectangles outlining the MS signal represent peak detection and their color coordination represents peak clustering.

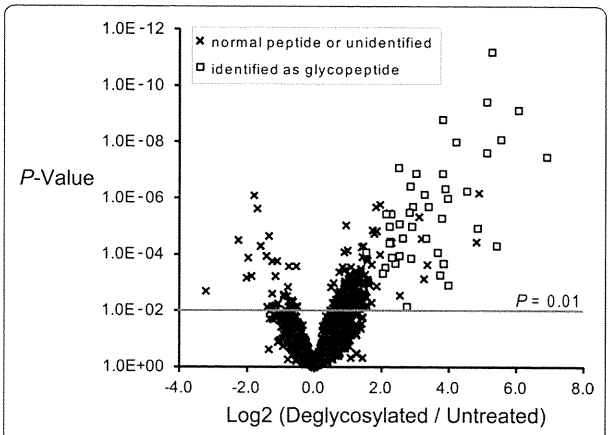

Figure 3 Volcano plot showing the difference in the peptide profiles of deglycosylated and untreated serum sample. Crosses represent peak clusters identified as normal peptides or not identified in the analysis, and squares represent deglycosylated peptides identified with +3 Da modification.

replicating runs was evaluated by calculating the correlation coefficients of the intensities of 2,356 clusters that were detected in all 12 runs. The correlation coefficients were calculated for all 15 possible combinations of 6 individual replicates within the experimental group. They ranged from 0.895 to 0.916 with mean value 0.899 (n = 15) in the untreated group and from 0.898 to 0.944 with mean value 0.914 (n = 15) in the deglycosylated group, suggesting that deglycosylation generally results in more reproducible data than the untreated (P < 0.002, t-test). Furthermore, coefficients of variation (CV) of the signal intensities for the same 2,356 peak clusters were calculated and compared between the two experimental groups (Figure 4). The frequency distribution of CV showed that deglycosylationtreatement resulted in slightly lowering the median CV from 34% to 31%. It is

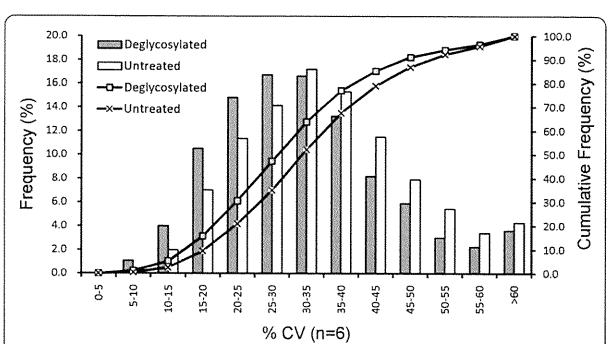

Figure 4 A frequency distribution plot of the coefficients of variations (CV) calculated for each of the 2,356 common peak clusters. Bars represent the frequency percentage and lines represent the cumulative frequency. Filled bars and boxes, replicates with deglycosylation; blank bars and crosses, untreated replicates (n = 6).

clear from these data that the effect of deglycosylation well extends to non-glycosylated peptides and enhances sensitivity and reproducibility.

Lung cancer biomarker screening

Deglycosylation-LC-MALDI platform was applied to the profiling of serum proteins for lung cancer biomarker screening. Control and lung cancer sera were immunodepleted, deglycosylated, purified on SDS-PAGE, in-gel digested and analyzed by LC-MALDI in the same way as described above. 30 mass chromatograms were processed simultaneously on Expressionist Refiner MS, and 23,453 peaks were detected, which were grouped into 6,186 peak clusters. Then we compared the two experimental groups, control (n = 10) and lung cancer (n = 20) by t-test and identified 63 peak clusters showing P < 0.01. In addition, 13 peak clusters were selected that have valid value of less than or equal to 2 in one experimental group and greater than 50% valid value proportion in the other. The total of 76 clusters was manually inspected and retrospective MS/MS was acquired by selecting the highest-expressing sample and the fraction spot of maximum elution for optimum MS/MS acquisition efficiency. As a result, 25 candidate proteins, comprising 40 candidate peptides, were identified (Table 1).

Next, these candidates were verified at peptide level by the MRM-based relative quantification analysis using the same preparation batch of serum tryptic digest as used for MALDI MS analysis as it is previously reported that LC-MALDI measurement is the most significant source of technical variability above sample preparation [16] (see Table S-3, Additional File 1 for the list of MRM transitions). This strategy was aimed at eliminating false-positive results from the long list of candidates and facilitating the selection of appropriate target for validation study. Of the 23 peptides that we found working MRM transitions, 11 peptides showed significant correlation (P < 0.05 by Pearson's correlation coefficient) in results obtained by MRM and MALDI MS, and 10 peptides (6 proteins) fulfilled P < 0.05 in both analyses. These peptide candidates were derived from ceruloplasmin, complement C3, complement component C9, inter-alpha-trypsin inhibitor heavy chain H3, inter-alpha-trypsin inhibitor heavy chain H4 and kininogen-1. The quantification results were summarized as dot-plots in Figure 5 to illustrate the potential performance of the 10 peptides as biomarker candidates. Raw data was normalized to the total detection and the samples were grouped as normal control, early stage (Stage I/II) and advanced stage (stage IIIb/IV) lung cancer cases. As the P-values indicate, most of the candidates showed significant response to cancer state even at early stages.

Further verification was performed by western blotting of complement C3 protein. Interestingly, expression of